Journal of Water Process Engineering 71 (2025) 107230

Contents lists available at ScienceDirect

Journal of Water Process Engineering

journal homepage: www.elsevier.com/locate/jwpe

A dynamic model for the prediction of malodorous compounds production from anaerobic methanogenic biofilm

Malek G. Hajaya [a], Rawan N. AlKaraki [b], Nataliia Kurnikova [c,d], Sergio Bordel [c,d], Raúl Muñoz [c,d,*]

[a] Department of Civil Engineering, Tafila Technical University, Tafila 66110, Jordan
[b] Department of Pharmaceutics and Pharmaceutical Technology, Mutah University, Alkarak 61710, Jordan
[c] Institute of Sustainable Processes, University of Valladolid, Dr. Mergelina, s/n, 47011, Valladolid, Spain
[d] Department of Chemical Engineering and Environmental Technology, School of Industrial Engineering, University of Valladolid, Dr. Mergelina, s/n, 47011, Valladolid, Spain

ARTICLE INFO

Editor: Li Gao

Keywords:
Integrated anaerobic biofilm reactor model
Methanogenesis
Multispecies biofilm model
Prediction of emissions
Sulphate reduction

ABSTRACT

A dynamic 1-D mathematical model for production and emission of a group of malodorous Volatile Sulphurous Compounds (VSCs) and volatile fatty acids from anaerobic microbial biofilms was herein formulated, calibrated, and validated. Mathematically, the biofilm was modelled using a multispecies approach, while microbial activity was modelled using the well-established Anaerobic Digestion Model 1 framework, amended with biochemical and physico-chemical processes to accurately represent the kinetics and compounds transportation in anaerobic methanogenic sulphate reducing biofilms. The model was formulated as an integrated Anaerobic Biofilm Reactor Model (ABRM) that provides a combined a dynamic output based on the processes taking place in the biofilm, liquid, and gas phases. Published experimental data representing the production of the targeted malodorous compounds obtained from a multi-reactor, lab-scale, anaerobic biofilm containing system fed with real wastewater was used to calibrate the model's parameters and to validate its predictions. ABRM predicted sulphite reduction and methanogenesis kinetics with R^2 values $\geq$0.916 and matched the trends of spatial and temporal variations of the experimental targeted malodorous compounds concentrations inside the reactors with Spearman's rank correlation coefficients $\geq$0.922. Simulation results for ABRM predicted spatial variations in the anaerobic biofilm's microbial species distribution, abundance, growth, substrate competition and uptake, hydrogen sulphate inhibition, and the levels of targeted malodorous compounds production and emissions in response to changes in operational conditions. In an integrated approach for odour control strategies, ABRM can play a great role in predicting malodorous emissions from microbial biofilms in wastewater treatment processes.

1. Introduction

Biofilms are aggregates of microorganisms and their extracellular polymers, naturally immobilized onto solid surfaces in layer-like assortments [1]. Biofilms are beneficial in a multitude of environmental applications, achieving a wide variety of desired treatment goals through engineered remediation and treatment processes. Among their prominent applications is their usage in wastewater treatment plants (WWTPs) [2]. To this end, biofilms are used in various configurations such as tricking filters, rotating biological contactors, membrane reactors, moving beds, fluidized beds, and anaerobic filters [3], facilitating the breakdown of pollutant through biodegradation, biomineralization, biosorption, and bioaccumulation [4]. Biofilm-based treatment processes are stable, simple, and reliable, mainly due to the resiliency and survivability provided by the biofilms [1].

Microbial biofilm's growth and development requires the presence of favourable environmental conditions such as pH, oxygen level, nutrient type and availability, and temperature [5]. Their minimum requirement for nutrients along with their ability to grow on a wide variety of biotic or abiotic, hydrophobic or hydrophilic surfaces increase their survivability and proliferation [6]. Therefore, microbial biofilms can appear ubiquitously, and sometimes uncontrollably, wherever such minimum requirements are met. On the other hand, uncontrolled biofilms usually represent an inhibitory and undesired component that can contaminate,

* Corresponding author at: Institute of Sustainable Processes, University of Valladolid, Dr. Mergelina, s/n, 47011, Valladolid, Spain.
E-mail address: raul.munoz.torre@uva.es (R. Muñoz).

https://doi.org/10.1016/j.jwpe.2025.107230
Received 12 December 2024; Received in revised form 19 January 2025; Accepted 8 February 2025
Available online 15 February 2025

hinder, and spoil equipment and environments [7]. In WWTPs, uncontrolled biofilms can corrode metals, reduce the lifetime of equipment, reduce the treatment efficiency, and introduce a variety of containments in the water stream and the atmosphere [8–10], causing a variety of process and material performance problems, in addition to health and aesthetic related issues [4]. In WWTPs, primary treatment is recognised as a major source of strong intensity odour [11,12], which are typically volatile, irritating even at low thresholds, and cause odour nuisance and discomfort [13]. The presence of anaerobic biofilms was found to exacerbate the problem of odorant compounds production in primary clarifiers [14], with biofilms mitigation actions specifically recommended to reduce odorant compounds production [15].

Volatile sulphur compounds (VSCs) and volatile organic carbon compounds (VOCs) are among the most typically recognised odour causing compounds [16]. VSCs include Hydrogen sulphide (H_2S) and Mercaptans (MT), while VOCs include a group of volatile fatty acids (VFAs) like acetic acid, propionic acid, butyric acid, and valeric acid [17–20]. These compounds can potentially occur simultaneously as a result of the metabolic activities in anaerobic biofilms, as they compete and utilize the same electron donors [21]. For instance, H_2S is produced through the biological reduction of sulphate (SO_4^{-2}) or thiosulfate by sulphate-reducing bacteria (SRB) in anaerobic environments [22], while the anaerobic degradation of sulphur-containing amino acids such as methionine and cysteine will generate H_2S and MT [23]. Similarly, VFAs are produced through fermentation of readily degradable organic compounds, and they are key intermediates in the process of methane (CH_4) production under anaerobic conditions [24].

The control of malodours emissions is one of the challenges facing WWTPs operators, as they represent an actual health related issue, and a nuisance that consistently give rise to complaints and lead to legal implications [10,11]. These challenges stem from the technical difficulties associated with their characterisation and monitoring, and their dynamic variation due to changes in WWTP's operational conditions and weather [25]. In this context, mathematical modelling is valuable tool that can be used to simulates the generation, dispersion, and concentration of odorous compounds in WWTP's, providing accurate predictions for their sources and quantities, and providing operators with targets that they can effectively intervene with effective treatment measures [26].

A multitude of modelling approaches for microbial biofilms has been discussed in the literature. Among which, one-dimensional (1-D) dynamic and steady-state models are widely used and implemented, as they represent a balance between simplified and complex modelling approaches [27]. This approach was also used in modelling anaerobic biofilms responsible for producing VSCs and/or VFAs. These models include: i) the Wastewater Aerobic/anaerobic Transformations in Sewers (WATS) model and its extensions [28–30], which is limited to sewer systems under steady state conditions, ii) the model developed by Sharma et al. [31], which dynamically simulate emissions related to aerobic, anoxic, and anaerobic transformations, with the inclusion of pH estimation in sewers. However, this model did not account for the presence of methanogenic activity, and approximated diffusional limitations in the biofilm by increasing the values of saturation constants; and iii) the model developed by Guisasola et al. [32], which extended the model presented by Sharma et al. [31] to include methanogenic activity in the biofilm, thus providing the ability to predict CH_4 emissions in sewers. Yet, the model neither considered the characteristics of the biofilm, apart from the surface area, nor included provisions to estimate emissions of malodorous VSCs and VFAs across the liquid-gas interface, thus limiting its application to operational conditions similar to those used in its development [32].

None of the previously discussed models included changes in the microbial community structure in their formulations. In this sense, establishing a basic understanding of the changes in the biofilm microbial structure, and the multitude of associated microbial activities in response to its surroundings, is important for the understanding of biofilm development and propagation. This knowledge can be instrumental in devising successful mitigation actions against it [33–36]. To satisfy this consideration, other models for anaerobic malodorous VSCs and VFAs producing biofilms did include the changes in microbial community structure in their formulations [21,37–39]. However, they did not include pH changes or transfer of malodorous VSCs and VFAs across the liquid-gas interface. Additionally, none of all discussed biofilm models included the provision to predict the production and emissions of MT.

This work aimed at developing a 1-D dynamic mathematical model that can simulate the production of a group of malodorous VSCs and VFAs resulting from anaerobic microbial biofilms. by combining relevant biofilm-associated biochemical and physico-chemical processes observed in the literature within the commonly adapted framework of the International Water Association (IWA) Anaerobic Digestion Model No. 1 (ADM1) [24]. The group of malodorous VSCs compounds include H_2S and MT, while the group of malodorous VFAs include acetate (Ac), propionate (Pro), valerate (Va), and butyrate (Bu). The developed model will be able to dynamically simulate the anaerobic biofilms response to changes in its surrounding conditions by predicting the influence of these changes on the biofilm's microbial species distribution and abundance, growth and activity, substrate uptake, and the levels of the targeted malodorous VSCs and VFA production. Furthermore, the model will be presented as an integrated anaerobic biofilm reactor model (ABRM) that provides a combined output based on the biochemical and physico-chemical process in the biofilm, liquid phase, and gas phase. This allows for its usage as a compartment in a Chemical Reactor Network (CRN) configuration, to accurately represent the prevailing hydrodynamic mixing conditions.

The developed ABRM will be calibrated and validated using literature sourced experimental data for a lab scale system for an anaerobic, methanogenic, sulphite reducing biofilm, fed with real wastewater. The model will also be used to obtain a basic understanding of the spatial variations in biofilm microbial structure along with the resulting microbial activities. This will be performed through operational simulations of the validated ABRM to reveal the microbial structure, biofilm characteristics, pH levels, and production levels of the targeted group of malodorous VSCs and VFA. In addition, the effect of changing the hydraulic retention time (HRT) on the level of malodorous VSCs and VFA production and emissions will be investigated.

Overall, this model delivers a clear picture for an important source of a group of malodorous VSCs and VFA emissions, providing information that are currently lacking in the field of predicting malodorous emissions production in WWTPs. The use of dynamic modelling will provide accurate odour assessment, while also improving understanding of the process of biofilm associated odorants formation. This is possible by including a multitude of aspects that are critical to the process such as material transport to and from the biofilm and across the liquid-gas interface, ability to predict changes in the biofilm characteristics (thickness and microbial community distribution) and activity, inclusion of a wide group of malodorous emissions causing compounds like H_2S, MT, and VFAs, pH estimation which affects important aspects like microbial inhibition and acid/base dissociation, and providing the ability to represent a wide range of hydrodynamics by adapting the CRN framework. Furthermore, the use of state-of-the art, commonly accepted and adapted variables of the ADM1 model will facilitate its inclusion in plant-wide simulations, thus reflecting operational changes on the level of malodorous air emissions. This will ultimately facilitate the adaptation of an integrated approach for odour control strategies in wastewater treatment processes, by using the model's outputs as inputs in air dispersion modelling.

2. Biofilm model formulation: The anaerobic biofilm reactor

In order to include the various dynamic interactions between the anaerobic biofilm and its surroundings, a three-phase biofilm reactor

framework was adapted [4]. The ABRM contains three phases: anaerobic biofilm phase, completely mixed liquid phase, and completely mixed gas phase. The anaerobic biofilm phase is comprised of active and inert biomass, it is fully submerged in the completely mixed liquid phase, with no direct contact between the biofilm phase and the gas phase. Transport of substrates and products to and from the biofilm is achieved through the completely mixed liquid phase. VSCs and VFA are transported to the gas phase through the liquid phase. Feed is introduced to and removed from the completely mixed liquid phase.

Adapting a biofilm reactor framework increases the model flexibility, as it allows for its adaptation within a CRN. This approach enables the integration of detailed chemical kinetics, involving multiple reactions, with a simplified flow representation. By breaking down complex systems into functional macro zones, known as compartments, various flow patterns can be effectively represented using combinations of ideal reactor flow models [40,41]. This allows for the representation of all possible flow conditions in WWTPs, accounting for their effect on the microbial biofilm [42].

The biological activity in the biofilm is assumed to be anaerobic and methanogenic. This is directly related to the targeted group of uncontrolled biofilms, which develop under conditions of stagnant, medium, or low flow conditions. These conditions will cause the formation of a boundary layer in the vicinity of the biofilm surface, drastically reducing or limiting oxygen from reaching the biofilm surface and creating a highly reduced environment suitable for anaerobic methanogenic and fermentative activity [43].

To this end, and to facilitate the usage of this model in plant-wide models, the biochemical and physico-chemical processes rates for anaerobic digestion developed in ADM1 are adapted in this model [24]. The model developed here is based on the mathematical treatment introduced by Rosen and Jeppsson for their ADM1 implementation within the Benchmark Simulation Model no. 2 (BSM2) Framework [44]. Both are discussed in detail in their referenced publications and won't be further discussed here. In this work, only changes/additions in the biochemical and physico-chemical processes and mathematical treatment discussed in BSM2 Framework [44] necessary to account for the formation of malodorous VSCs and VFAs in an anaerobic methanogenic multispecies biofilm are discussed.

Following the nomenclature in ADM1, S represent a dissolved substance concentration, X represent particulate matter concentration. For compounds that are made up by an acid/base pair, the model follows their total concentrations. Active microbial species assumed present in the biofilm are: monosaccharides (Su) degraders (X_{su}), amino acids (AA) degraders (X_{AA}), long-chain fatty acids (Fa) degraders (X_{fa}), Va and Bu (Bu) degraders (X_{c4}), dissolved Pro degraders (X_{Pro}), dissolved Ac degraders (X_{ac}), and dissolved hydrogen (H_2) degraders (X_{H2}). The introduced SRB are Pro utilizing SRB ($X_{SRB,Pro}$), Ac utilizing SRB ($X_{SRB,Ac}$), and H_2 utilizing SRB ($X_{SRB,H2}$) [45–49]. Additionally, inert biomass in the biofilm is assumed to be in the form of inert particulate matter.

2.1. Biochemical processes

In the biofilm reactor model, biological activity is assumed to be only found in the biofilm phase. This assumption is backed by the fact that in sewer systems, were environmental conditions similar to the ones behind anaerobic methanogenic biofilm proliferation exist, biofilms are the main contributors to H_2S and CH_4 producing biological activity, with negligible contribution from suspended microorganisms [32].

ADM1 specifies the following biochemical process rates: disintegration, hydrolysis, uptake, inhibition, and inactivation/decay, [24,44]. In the ABRM, modifications and additional bioprocesses are added to the aforementioned ADM1 processes, these are discussed in the subsequent sections.

2.1.1. Disintegration and hydrolysis

Disintegration and hydrolysis are the two biochemical processes associated with the transformation and production of particulate compounds. These particulate compounds include degradable composite particulates (X_C), inert particulates (X_I), particulate carbohydrates (X_{Ch}), particulate proteins (X_{Pr}), and particulate fats (X_{Fa}). The disintegration process of degradable composite particulates directly produces X_I, X_{SU}, X_{Pr}, and X_{Fa}, along with dissolved inert (S_I). While the hydrolysis process converts X_{Ch}, X_{Pr}, and X_{Fa} to S_{Su},S_{AA}, and S_{fa}. In the liquid phase of the ABRM, the ADM1 approach for these two processes is adapted.

As for the production of X_C, two modifications are introduced. In the liquid phase, X_C is no longer produced by microbial inactivation/decay process as assumed in ADM1. Instead, it is assumed that X_C is produced through the biofilm detachment process. To represent this additional process, the detachment velocity of biomass between the biofilm and liquid phases and the biomass transport through detachment are defined [50,51]:

$$f_i(t,z) = \frac{V_{i,f}}{V_f} \tag{1}$$

$$X_{i,f}(t,z) = X_f f_i(t,z) \tag{2}$$

$$\sigma(t,z) = k_{det}\left[L_f(t,z)\right]^2 \tag{3}$$

$$\rho_{20,i} = \sigma(t,z) X_f(t,z) f_i(t,z) \frac{A_f}{V_B} \tag{4}$$

where f_i is the biofilm volume fraction of the microbial species i in the biofilm top layer (biofilm/liquid interface), V_f is the biofilm phase volume (m^3), $V_{i,f}$ is the volume occupied by species i in the biofilm (m^3), X_i biomass concentration in the biofilm for species i ($\frac{kg\ COD}{m^3}$), X_f is the biomass density in the biofilm, assumed constant and equal for all species ($\frac{kg\ COD}{m^3}$), σ is the detachment velocity of biomass between biofilm (f) and liquid (b) phases ($\frac{m}{d}$), k_{det} is the detachment coefficient ($\frac{1}{d.m}$), L_f is the biofilm thickness (m), $\rho_{20,i}$ the particulate matter transport through detachment of species i from the biofilm top layer (biofilm/liquid interface) to the liquid phase ($\frac{kg\ COD}{d.m^3}$), A_f surface area of biofilm phase in contact with liquid phase (m^2), and V_B is the completely mixed liquid phase volume (m^3).

In the second modification of the model herein developed, disintegration and hydrolysis are combined in one process that depends on the microbial inactivation/decay rate [52–54]. By this assumption, production of S_{Su},S_{AA}, S_{fa}, and dissolved inerts (S_I), and X_I in the biofilm is equated to the microbial inactivation/decay, each through their ADM1 stoichiometric parameter. Eqs. (5)–(8) are based on the processes defined in BSM2 [44]:

$$\rho_{1,f} = \sum_{i=1}^{n}\left(X_{i,f}(t,z) k_{d,i,f}\right) = X_f \sum_{i=1}^{n}\left(f_i(t,z) k_{d,i,f}\right) \tag{5}$$

$$\rho_{2,f} = f_{ch,xc} X_f \sum_{i=1}^{n}\left(f_i(t,z) k_{d,i,f}\right) \tag{6}$$

$$\rho_{3,f} = f_{pr,xc} X_f \sum_{i=1}^{n}\left(f_i(t,z) k_{d,i,f}\right) \tag{7}$$

$$\rho_{4,f} = f_{li,xc} X_f \sum_{i=1}^{n}\left(f_i(t,z) k_{d,i,f}\right) \tag{8}$$

where $\rho_{1,f}$, $\rho_{2,f}$, $\rho_{4,f}$, and $\rho_{4,f}$ are combined disintegration and hydrolysis processes in the biofilm ($\frac{kg\ COD}{d.m^3}$), n is the number of active microbial species in the biofilm, $k_{d,i,f}$ is the 1st order inactivation/decay rate constant in the biofilm adapted from ADM1 ($\frac{1}{d}$), and $f_{i,xc}$ is the ADM1

stoichiometric parameter for the production of i from X_C in the biofilm.

2.1.2. Substrate uptake

To incorporate the activity of the three types SRBs, three additional rates are required (Eqs. (9)–(11)). Using a multi substrate Monod equation, the biochemical process of SO_4^{-2} reduction by SRB utilizing substrate i in the biofilm can be formulated as follows [45,55,56]:

$$\rho_{10,SRB} = k_{m,SRB,Pro}\frac{S_{Pro,f}}{S_{Pro,f}+K_{S,SRB,Pro}}\frac{S_{SO4,f}}{S_{SO4,f}+K_{S,SO4,Pro}}X_{SRB,Pro}I_{Pro,H2S,SRB} \quad (9)$$

$$\rho_{11,SRB} = k_{m,SRB,Ac}\frac{S_{Ac,f}}{S_{Ac,f}+K_{S,SRB,Ac}}\frac{S_{SO4,f}}{S_{SO4,f}+K_{S,SO4,Ac}}X_{SRB,Ac}I_{Ac,H2S,SRB} \quad (10)$$

$$\rho_{12,SRB} = k_{m,SRB,H2}\frac{S_{H2,f}}{S_{H2,f}+K_{S,SRB,H2}}\frac{S_{SO4,f}}{S_{SO4,f}+K_{S,SO4,H2}}X_{SRB,H2}I_{H2,H2S,SRB} \quad (11)$$

where $\rho_{10,SRB}$, $\rho_{11,SRB}$, and $\rho_{12,SRB}$ are uptake of Pro, Ac, and H_2, respectively by SRB activity ($\frac{kg\ COD}{d.m^3}$), $k_{m,SRB,i}$ is the maximum uptake rate for substrate i (i = Pro, Ac, and H_2) ($\frac{1}{d}$), $K_{S,SRB,i}$ is the half saturation rate constant for substrate i for SO_4^{-2} reduction ($\frac{kg\ COD}{m^3}$), $S_{SO4,f}$ SO_4^{-2} biofilm concentration (M), $K_{S,SO4,i}$ is the half saturation rate constant for SO_4^{-2} reduction for substrate i (M), and $I_{i,H2S,SRB}$ is free H_2S inhibition for SO_4^{-2} reduction utilizing substrate i. Free H_2S inhibition is represented by Eq. (12):

$$I_{i,H2S,SRB} = 1 - \frac{S_{H2S,f}^{free}}{K_{I,H2S,j}} \quad (12)$$

where $S_{H2S,f}^{free}$ is the biofilm free H_2S concentration (M) and $K_{I,H2S,j}$ is free H_2S inhibition constant for bioprocess j (M). Free H_2S inhibition also affects the uptake of S_{Ac}, and S_{H2} (methanogenesis). The same inhibition function is used for the anaerobic digestion bioprocesses (ρ_5 to ρ_{12}) [55], but with different inhibition coefficients that reflects the difference in free H_2S susceptibility.

To complete the bioprocesses required for the representation of SRB activity in the biofilm, inactivation/decay rates are also added (Eq. (13)). These follow the same 1st order equations used in ADM1 and contribute to the process in Eq. (5):

$$\rho_{i,SRB} = X_f f_i(t,z) k_{d,i,SRB} \quad (13)$$

where $\rho_{i,SRB}$ is the inactivation/decay process and $k_{d,i,SRB}$ is the inactivation/decay coefficient for SRB (i: 17, 18, and 19 corresponding for Pro, Ac, and H_2, respectively).

Another bioprocess associated with malodorous VSCs production is the release of H_2S and MT as a result of the uptake of sulphur containing AA [45]. To include their production in the biofilm, H_2S and MT are assumed to be produced by the uptake of AA (ρ_6 in BSM2) in a stoichiometric ratio similar to their content in AAs [57]. Table 1 lists the stoichiometric parameters, and the biochemical processes added to the ADM1 model.

2.2. Physico-chemical processes

The physico-chemical processes in ABRM include pH calculation, acid/base dissociation, and solid/liquid and liquid/gas transfer processes. These are non-biologically driven processes that are assumed to take place only in the liquid phase.

2.2.1. pH calculations

Previously published results showed that pH value inside biofilms showed an insignificant gradient in anaerobic methanogenic biofilms with measured values inside the biofilm close to those in the liquid phase [21,49]. Moreover, additional studies showed that pH can be calculated sufficiently based on the liquid phase [58,59]. Therefore, it is assumed that no pH gradient occurs within the biofilm, and its value throughout the biofilm is identical to the value of the liquid phase, where it will be evaluated. To calculate pH in the liquid phase of the biofilm reactor, the same approach in BSM2 is used [44]. The approach includes using an algebraic equation based on the electroneutrality principle to evaluate pH as a function of the concentration of ionic species in the liquid phase. For this model, concentrations of bisulfide (HS^-) and SO_4^{-2} are added to the pH equation.

2.2.2. Acid/base rates

The ABRM followed the Ordinary Differential Equations (ODE) approach used in ADM1 to evaluate the concentration of the ionic species in the liquid phase. This approach expresses the acid/base reactions as processes rates that represent the production/consumption of ionic species [44]. The model includes all the acid/base rates in BSM2 with an added acid/base rate for H_2S (Eq. (14)):

$$\rho_{A,12} = k_{\frac{A}{B},H2S}\left[S_{HS-,b}(t)\left(K_{a,H2S}+S_{H+,b}(t)\right) - K_{a,H2S}S_{H2S,b}(t)\right] \quad (14)$$

where $\rho_{A,12}$ is the acid/base rate for H_2S ($\frac{1}{d}$), $S_{HS-,b}$ is HS^- concentration (M), $k_{\frac{A}{B},H2S}$ is the ADM1 acid/base rate constant; ADM1 suggested default value = 1×10^8 ($\frac{1}{d.M}$), $K_{a,H2S}$ is the acid base dissociation constant for H_2S, $S_{H+,b}$ is hydrogen ion concentration in the liquid phase (M), and $S_{H2S,b}$ is the total H_2S concentration (M). For H_2SO_4/ HSO_4^-/SO_4^{-2} speciation, SO_4^{-2} is assumed to be the only species present in the biofilm reactor. Finally, the concentration of ionic state dependant species (Ammonia, unprotonated H_2S, and dissolved carbon dioxide (CO_2)) in the biofilm are calculated based on the total concentration of the species and the liquid phase pH, assuming instantaneous equilibrium between the ionic states.

2.2.3. Biofilm-liquid transport process rates

Transport of compounds between the biofilm and liquid phases is assumed to be governed by mass transfer limitations. This is directly related to the targeted group of uncontrolled biofilms in this model, which develop under conditions of stagnant, medium, or low flow conditions. These conditions will cause the formation of a boundary layer in the vicinity of the biofilm surface, drastically reducing or limiting material transport to and from the biofilm [43]. This process is not found in ADM1, and it's added for all the compounds transported to and from the biofilm. The rate of material transport process between the biofilm and liquid phases for compound i can be represented as follows (Eq. (15)):

$$\rho_{BT,i} = \frac{A_f}{V_b R_{L,i}}\left[S_{i,b}(t) - S_{i,f}(t,L_f)\right] \quad (15)$$

where $\rho_{BT,i}$ is the rate of material transport process between the biofilm and liquid phases for compound i ($\frac{kg\ COD}{d.m^3}$ *or* $\frac{kmol}{d.m^3}$), $R_{L,i}$ is the mass transfer resistance external to the biofilm for i ($\frac{1}{m}$), and $S_{i,b}$ and $S_{i,f}$ *at* L_f are substrate/product i concentrations in the bulk liquid phase, and the outer layer of the biofilm, respectively ($\frac{kg\ COD}{m^3}$ *or* $\frac{kmol}{m^3}$). $R_{L,i}$ can be evaluated using Eq. (16) [4]:

$$R_{L,i} = \frac{L_L}{D_{i,w}} \quad (16)$$

where L_L is the thickness of the mass transfer boundary layer (m) and $D_{i,w}$ is the diffusion coefficient of the transported constituent i in water ($\frac{m^2}{d}$). In this model, L_L is treated as a fitting parameter [60], with a value of 10 % of the biofilm thickness.

2.2.4. Liquid-gas transport process rates

Transport of compounds between the liquid and gas phases is represented in ADM1, but only for CO_2, H_2, and CH_4. To represent the

Table 1
The stoichiometric parameters and the biochemical processes added to the ADM1 model.

Process	Eq.	$S_{su,f}$	$S_{AA,f}$	$S_{Fa,f}$	$S_{I,f}$	$S_{Pro,f}$	$S_{Ac,f}$	$S_{H2,f}$	$S_{H2S,f}$	$S_{MT,f}$	$S_{SO4,f}$	$X_{C,b}$	$X_{I,f}$	$X_{SRB,Pro}$	$X_{SRB,Ac}$	$X_{SRB,H2}$
$\rho_{1,b}$	Eq. 30											−1				
ρ_{20}	Eq. 4											$\sum_{i=1}^{n} \rho_{20,i}$				
$\rho_{1,f}$	(5)				$f_{SI,xc}$								$f_{XI,xc}$			
$\rho_{2,f}$	(6)	1														
$\rho_{3,f}$	(7)		1													
$\rho_{4,f}$	(8)	$1 - f_{fa,li}$		$f_{fa,li}$												
$\rho_{6,f}$	Eq. 26		−1			$(1 - Y_{Pro,aa})f_{Pro,aa}$	$(1 - Y_{Ac,aa})f_{Ac,aa}$	$(1 - Y_{H2,aa})f_{H2,aa}$	$(1 - Y_{aa})f_{H2S,aa}$ [a]	$(1 - Y_{aa})f_{Mt,aa}$ [b]	–					
$\rho_{10,SRB}$	Eq. 9					−1	1		$\left[\frac{0.75}{112}\right]^{c}(1 - Y_{pro,SRB}) - Y_{pro,SRB}S_{bio}$		$-\left[\frac{0.75}{112}\right](1 - Y_{pro,SRB})$			$Y_{pro,SRB}$		
$\rho_{11,SRB}$	Eq. 10						−1		$\left[\frac{1}{64}\right](1 - Y_{Ac,SRB}) - Y_{Ac,SRB}S_{bio}$ [d]		$-\left[\frac{1}{64}\right](1 - Y_{Ac,SRB})$				$Y_{Ac,SRB}$	
$\rho_{12,SRB}$	Eq. 11							-1	$\left[\frac{1}{64}\right](1 - Y_{H2,SRB}) - Y_{H2,SRB}S_{bio}$		$-\left[\frac{1}{64}\right](1 - Y_{H2,SRB})$					$Y_{H2,SRB}$
$\rho_{17,SRB}$	Eq. 13													−1		
$\rho_{18,SRB}$															−1	
$\rho_{19,SRB}$																−1

a: $f_{H2S,aa}$: stoichiometric parameter of H_2S from AA uptake; b: $f_{Mt,aa}$: stoichiometric parameter of MT from AA uptake; c: stoichiometric yield based on the SO_4^{-2} reduction biochemical reaction; d: Sulphur content in biomass.

emissions of malodorous VSCs and VFAs, the following transfer rate is introduced in the biofilm model following the same approach in BSM2 [44] for the included VSCs and VFA (Eqs. (17)–(18)):

$$\rho_{T,i} = K_{la,i}\left(S_{i,b}(t) - K_{H,i}P_{i,g}(t)f_{COD}\right) \tag{17}$$

$$P_{i,g}(t) = K_{H,i}S_{i,g}(t)\frac{RT}{f_{COD}} \tag{18}$$

where $\rho_{T,i}$ is the liquid gas transfer process for compound i ($\frac{kg\ COD}{d.m^3}$ *or* $\frac{kmol}{d.m^3}$), i is 4 for Va, 5 for Bu, 6 for Pro, 7 for Ac, 12 for H_2S, and 13 for MT, $K_{la,i}$ is volume specific liquid-gas transfer coefficient ($\frac{1}{d}$), $K_{H,i}$ is Henry's law coefficient ($\frac{M}{bar}$), $S_{i,g}$ is compound i gas phase concentration ($\frac{kg\ COD}{m^3}$ *or* $\frac{kmol}{m^3}$), R is the universal gas constant (0.083145 $\frac{bar}{MK}$), T is the absolute temperature (K), $P_{i,g}$ compound i gas phase pressure (bar), and f_{COD} is the chemical oxygen demand (COD) equivalent per mole to convert the concentration from $\frac{kg\ COD}{m^3}$ *to* $\frac{kmol}{m^3}$ when needed, else = 1 [44]. It must be added that for acid/base forming compounds, $S_{i,b}$ represents the free, unprotonated form.

2.3. Biofilm phase equations

In this model, the microbial activity in the ABRM is assumed to be limited to the biofilm, with negligible biological activity in the bulk liquid phase. Biomass growth, substrate/product transport, and biofilm thickness were modelled using the multispecies biofilm model approach [50]. The biofilm phase equations include the equation for the multi-species biofilm model and the equations for dissolved compounds in the biofilm.

2.3.1. The multispecies biofilm model

The biofilm phase is modelled as a multi-species1-D biofilm. The 1-D representation is considered sufficient for engineering application [61]. For active microbial species i in the biofilm, the following Eqs. (19)–(23) can be formulated following the mass balance approach:

$$\frac{\partial f_i(t,z)}{\partial t} = f_i(t,z)\left[\mu o_{i,f}(t,z) - \overline{\mu o}\ (t,z)\right] - u(t,z)\frac{\partial f_i(t,z)}{\partial z} \tag{19}$$

$$\overline{\mu o}\ (t,z) = \sum_{i=1}^{n}\mu o_{i,f}(t,z)f_i(t,z) \tag{20}$$

$$u(t,\acute{z}) = \int_0^{\acute{z}}\overline{\mu o}(t,\acute{z}d\acute{z} \tag{21}$$

$$u_L(t) = \int_0^{L_f}\overline{\mu o}\ (t,z)\ dz - \sigma(t) \tag{22}$$

$$\frac{dL_f}{dt} = u_L(t) \tag{23}$$

where $\mu o_{i,f}$ and $\overline{\mu o}$ are net and mean specific growth and conversion rates in the biofilm for species i ($\frac{1}{d}$), respectively, n is the number of species in the biofilm (including inert biomass), u is the velocity at which the microbial mass is displaced with respect to the film-support interface at point $\acute{z}$ in biofilm ($\frac{m}{d}$), and u_L is the velocity of the biofilm-water interface ($\frac{m}{d}$).

The boundary condition required to solve the previously discussed system is obtained by the no biomass flux condition at the substratum (i.e. $u = 0$) [50] (Eq. (24)):

$$\text{at } z = 0, \frac{\partial f_i(t,0)}{\partial t} = f_i(t,z)[\mu o_i(t,o) - \overline{\mu o}\ (t,o)\ ] \tag{24}$$

In this model, inert particulate compounds are included in the multi-species biofilm model as a microbial species. These compounds are assumed to be produced from the simultaneous disintegration and hydrolysis of degradable particulate compounds in the biofilm (Section 2.1.1).

2.3.2. Soluble material equations

The following Eqs. (25)–(27) can be obtained for any substrate/product i in the biofilm, assuming diffusive transport:

$$\frac{\partial S_{i,f}(t,z)}{\partial t} = D_i\frac{\partial^2 S_{i,f}(t,z)}{\partial z^2} + r_{i,f}(t,z) \tag{25}$$

$$r_{i,f}(t,z) = \sum_{j=1}^{m}\rho_{j,f}(t,z)\nu_{ij} \tag{26}$$

$$\mu o_{i,f}(t,z) = \sum_{j=1}^{m}\frac{\rho_{j,f}(t,z)\nu_{ij}}{X_{i,f}(t,z)} \tag{27}$$

where $S_{i,f}$ is substrate/product total concentration ($\frac{kg\ COD}{m^3}$ *or* $\frac{kmol}{m^3}$), D_i is the diffusion coefficient in the biofilm ($\frac{m^2}{d}$), assumed to be 90 % of $D_{i,w}$ [60], $r_{i,f}$ is the observed uptake rate of substrate i ($\frac{kg\ COD}{d\ m^3}$ *or* $\frac{kmol}{d\ m^3}$), m is the number of processes associated with substrate i in the biofilm, $\rho_{j,f}$ is the biochemical process rate j in the biofilm ($\frac{kg\ COD}{d\ m^3}$ *or* $\frac{kmol}{d\ m^3}$), and ν_{ij} is the stoichiometric coefficient for substrate/product i in process j. Two boundary conditions are required to solve the previous system (Eqs. (28) and (29)):

$$\text{at } z = 0, \frac{\partial S_{i,f}(t,0)}{\partial z} = 0 \tag{28}$$

$$\text{at } z = Lf, \frac{\partial S_{i,f}\left(t,L_f\right)}{\partial z} = R_{L,i}\left[S_{i,b}(t) - S_{i,f}\left(t,L_f\right)\right] \tag{29}$$

where $S_{i,b}$ and $S_{i,f}$ *at* L_f are substrate/product i concentrations in the bulk liquid phase, and the outer layer of the biofilm ($\frac{kg\ COD}{m^3}$ *or* $\frac{kmol}{m^3}$). The boundary condition in Eq. (29) was chosen to reflect the presence of a mass transfer boundary layer, which represent a more realistic situation in the case of anaerobic biofilms [4]. Transport of inert dissolved compounds is included in the multi-species biofilm model. Their conversion rate is assumed to be associated to the simultaneous disintegration and hydrolysis of degradable particulate compounds in the biofilm (Section 2.1.1).

2.4. The liquid phase

The liquid phase is assumed to be a completely mixed compartment with constant volume, and the biofilm volume increase due to microbial growth is assumed to be negligible. The liquid phase equations include equations for the concentrations of suspended particulate matter and dissolved compounds in the liquid phase (targeted groups VSC's and VOCs included).

2.4.1. Particulate material equations

Particulate material in the liquid phase of the biofilm reactor includes degradable composite particulates (X_C), inert particulates (X_I), particulate carbohydrates (X_{Ch}), particulate proteins (X_{Pr}), and particulate fats (X_{Fa}). As discussed in Section 2.1.1, biofilm detachment is the only contributor to degradable composite particulates (X_C). Thus, using mass balance for a constant volume, Eq. (30) for X_C can be written as:

$$\frac{\partial X_{C,b}(t)}{\partial t} = \frac{q_L}{V_b}\left(X_C^o(t) - X_{C,b}(t)\right) + \sum_{i=1}^{n}\rho_{20,i}(t) - \rho_{1,b} \tag{30}$$

where X_C^o and $X_{C,b}$ are degradable composite particulates concentration in the feed and liquid phase, respectively ($\frac{kg\ COD}{m^3}$), q_L is the biofilm reactor liquid feed and effluent flow rate ($\frac{m^3}{d}$), n is the number of active

microbial species in the top layer of the biofilm, and $\rho_{1,b}$ is the liquid phase disintegration rate ($\frac{kg\ COD}{d.m^3}$). The remaining particulate matter equations were adapted from BSM2 [44].

2.4.2. Soluble matter equations: Substrates and products

Transport of dissolved soluble matter between the liquid phase and biofilm phase is governed by mass transfer limitations. Material flux is quantified as an average over the contact surface area between the biofilm and the liquid phase. The concentration of dissolved compounds in the liquid phase can be represented by the following Eq. (31):

$$\frac{\partial S_{i,b}(t)}{\partial t} = \frac{q_L}{V_b}\left(S_i^o(t) - S_{i,b}(t)\right) + r_{i,b}(t) + \rho_{BT,i} - \rho_{T,i} \tag{31}$$

where $S_{i,b}$ and S_i^o are substrate/product total concentration in the liquid phase and in the feed flow rate ($\frac{kg\ COD}{m^3}$ *or* $\frac{kmol}{m^3}$), $r_{i,b}$ is the observed non-biological conversion rate of substrate i ($\frac{kg\ COD}{d\ m^3}$ *or* $\frac{kmol}{d\ m^3}$), and $\rho_{BT,i}$ and $\rho_{T,i}$ are biofilm-liquid and liquid-gas transport for substrate i, respectively ($\frac{kg\ COD}{dm^3}$ *or* $\frac{kmol}{dm^3}$). Either one the transport processes $\rho_{BT,i}$ and $\rho_{T,i}$ can be included or excluded depending on the assumed fate of the compound in ABRM.

2.4.3. Soluble matter equations: Inorganic carbon and nitrogen

In the original ADM1, the material balance on the concentrations of inorganic carbon ($S_{IC,b}$) in the liquid phase include provisions to calculate the net effects of substrate uptake (due to microbial activity) and the inactivation/decay process on inorganic carbon material balance [24]. In addition, for inorganic nitrogen ($S_{IN,b}$), the net effect of the inactivation/decay process and the disintegration process are also included.

In the ABRM, substrate uptake ($r_{i,f}(t,z)$) and the process of inactivation/decay take place only in the biofilm and thus varies with its depth. Therefore, in this model the net effect of substrate uptake is evaluated through the rate of biofilm-liquid transport process for that substrate ($\rho_{BT,i}$) [1]. While the net effect of the process of inactivation/decay is evaluated by integrating the localized inactivation/decay rates over the biofilm thickness. Additionally, to account for inorganic carbon and nitrogen resulting from the disintegration process, the disintegration rate is also added ($\rho_{20,i}$). Therefore, assuming no mass transfer limitations on inorganic carbon and inorganic nitrogen and adapting the approach in BSM2, the equation (Eq. (32)) of inorganic carbon concentration in the liquid phase can be written as follows:

$$\frac{\partial S_{IC,b}(t)}{\partial t} = \frac{q_L}{V_b}\left(S_{IC}^o(t) - S_{IC,b}(t)\right) - \left[\sum_{i=1}^{m} s_i \rho_{BT,i}(t) + s_{13}\sum_{i=1}^{n}\left(X_f \int_0^{L_f(t)} f_i(t,z) k_{di,f}\, dz + \rho_{20,i}\right)\right] - \rho_{T,CO2} \tag{32}$$

where S_{IC}^o and $S_{IC,b}$ are inorganic carbon concentration in the feed and liquid phase ($\frac{kmol}{m^3}$), i is the number of biochemical uptake processes in the biofilm, and n is the number of active microbial species in the biofilm.

The equation for inorganic nitrogen concentration in the liquid phase can be used as found in BSM2 [44], with the following term replaced to calculate the net effect of inactivation/decay (Eq. (33)):

$$\sum_{k=13}^{19}(\rho_k) = \sum_{i=1}^{n}\left(X_f \int_0^{L_f(t)} f_i(t,z) k_{di,f}\, dz + \rho_{20,i}\right) \tag{33}$$

And the following term added to account for the instantaneous disintegration in the biofilm, as shown in Section 2.1.1 Eq. (5):

$$\rho_1 = \rho_{1,b} + \sum_{i=1}^{n}\left(X_f \int_0^{L_f(t)} f_i(t,z) k_{di,f}\, dz\right) \tag{34}$$

where ρ_k is the inactivation/decay process for microbial species k in BSM2, and ρ_1 is the liquid phase disintegration rate.

2.4.4. Soluble matter equations: Ionic species

Following the ODE approach used in BMS2 [44], the following equation can be used to evaluate the concentration of the ionic species i in the liquid phase.

$$\frac{\partial S_{i,b}(t)}{\partial t} = -\rho_{A,i} \tag{35}$$

In addition to all the ionic species found in ADM1, another equation for HS^- was added with the acid/base rate for H_2S ($\rho_{A,12}$).

2.5. The gas phase

In the biofilm reactor, malodorous VSCs and VFAs are produced in the biofilm, transported through the liquid phase, and emitted to the gas phase. Following the treatment found in ADM1 [44], the fate of compound i in the gas phase can be described by Eq. (36):

$$\frac{\partial S_{i,g}(t)}{\partial t} = -\frac{q_G}{V_g} S_{i,g}(t) + \rho_{T,i}\frac{V_b}{V_g} \tag{36}$$

where V_g is the liquid phase volume (m^3) and q_G is the gas flow rate ($\frac{m^3}{d}$) [44], the latter defined by Eq. (37):

$$q_G(t) = \frac{RT}{p_{atm} - pg_{H2O}} V_b \left(\sum_{i=1}^{n}\frac{\rho_{T,i}(t)}{f_{COD}}\right) \tag{37}$$

where p_{atm} and pg_{H2O} are the atmospheric and water vaper pressures (bar), and n is the number of volatile compounds. Total gas pressure in the headspace can be calculated using Eq. 38:

$$P_{G,Total}(t) = \left(\sum_{i=1}^{n} P_{i,g}(t)\right) \tag{38}$$

where $P_{G,Total}$ is the total pressure in the head space (*bar*). Finally, in situations where the no gas phase is present in the ABRM, the gas phase could be eliminated along with its associated processes present in other sub-models (i.e. liquid-gas transport). In this case the ABRM will provide the liquid phase concentrations of the targeted VSCs and VFAs.

2.6. Model calibration, verification, and simulation

2.6.1. Experimental data

The ABRM is formulated to be able to simulate anaerobic biofilms response to prevailing environmental and operational conditions. This will be performed by predicting their influence on the microbial species distribution and abundance, growth and activity, substrate uptake, and the production levels of the targeted VSCs and VFAs in the anaerobic biofilm.

To calibrate and validate the model, experimental data were obtained from a lab-scale sewer system that contained an anaerobic methanogenic biofilm [32]. The lab scale model comprised from four CSTRs (RM1, RM2, RM3, and RM4) connected in series, fed with real wastewater, closed with no headspace, and each contained an anaerobic methanogenic biofilm covering the interior (top and walls) with an area/volume ratio of 56.7 m^2/m^3. The system represented a pipe section in a sewer pipeline and was fed sequentially (7.6×10^{-4} (m^3) 16 times a day) with real screened and settled wastewater to simulate the flow conditions in real sewers. The HRT for the system ranged between 2 and 10 h, with an average value of 6 h. Additional details of the system can be found in the cited paper.

The data showed two experimental case studies: The first case study represented 4 batch tests (for 7 h) for each reactor after extended operation and biofilm growth, with time course data for dissolved degradable COD concentration, S_{SO4}, S_{H2S}, S_{Ac}, S_{Pro}, and S_{CH4} inside each reactor, that showed the rate of substrates uptake and products formation in all reactors. The second case study depicted the daily operation of

two reactors (RM2 and 3), with data for the time course concentration for S_{SO4}, S_{H2S}, total dissolved VFA's concentrations (S_{VFAs}), and S_{CH4}, during 10 feed pumping events at different time intervals. The second data set showed the performance under varying HRT and revealed the presence of spatial variation in biofilm activity between the two reactors. All the experiments were conducted at 23 °C, and data was provided for the system size, and wastewater flowrate. Batch tests were conducted after the full development of the biofilm inside the reactors.

While the anaerobic reactor model uses the ADM1 units for concentrations i.e. $\frac{kg\ COD}{m^3}$ and $\frac{kg\ mole}{m^3}$, results will be given in concentration units similar to the experiential data i.e. $\frac{mg\ COD}{L}$, $\frac{mg}{L}$, and $\frac{\mu g}{L}$. The screened and settled wastewater was reported to contain the following: dissolved degradable COD = 135 $\left(\frac{mg\ COD}{L}\right)$, S_{SO4}= 15 $\left(\frac{mg-S}{L}\right)$, S_{H2S} = negligible, S_{Ac}=50 $\left(\frac{mg\ COD}{L}\right)$, S_{Pro}=15 $\left(\frac{mg\ COD}{L}\right)$, and $S_{CH4} \leq 5$ $\left(\frac{mg\ COD}{L}\right)$.

In the cited paper [32], the data was used to amend the previously published model by Sharma et al., 2008 [31] with the processes of methane production in sewer lines. While being successful in their purpose, successfully simulating the dynamic production of H_2S and CH_4, establishing the characteristics of the biofilm such as its microbial structure and associated activity and predicting the transfer of malodorous VSCs s and VFAs across the liquid-gas interface were beyond its scope.

2.6.2. ABRM calibration and validation

The experimental data discussed in Section 2.6.1 provided an opportunity to not only validate the bioreactor model but also test its flexibility. Apart from its surface area, minimum information is provided about the biofilm inside the system. No data was provided regarding the biofilm's microbial species distribution, thickness, detachment rate, or biomass concentration. pH changes inside the system were not provided, and no gas emission rates were reported, as the system did not have a gas phase. In addition, the feed wastewater characteristics were limited to dissolved COD, two VFA's (propanoate and acetate), SO_4^{-2}, and H_2S.

To test the bioreactor model flexibility, the limited experimental data was used to calibrate the ABRM, specifically the batch study data for one of the reactors (RM1). However, another complication resulted from the fact that no clear indication is given for the time period required to reach a fully developed anaerobic biofilm, beyond being “after several months”. This time period is important as it sets the initial conditions for the batch test simulations. To this end, the calibration processes included the identification of that time period, and it was determined by reaching a steady biofilm thickness inside all four reactors. This time period was assumed to not exceed 7 months. Additionally, to reduce the computing time and excess complexity, the operation of the lab scale system to reach the fully developed anaerobic biofilm was simulated

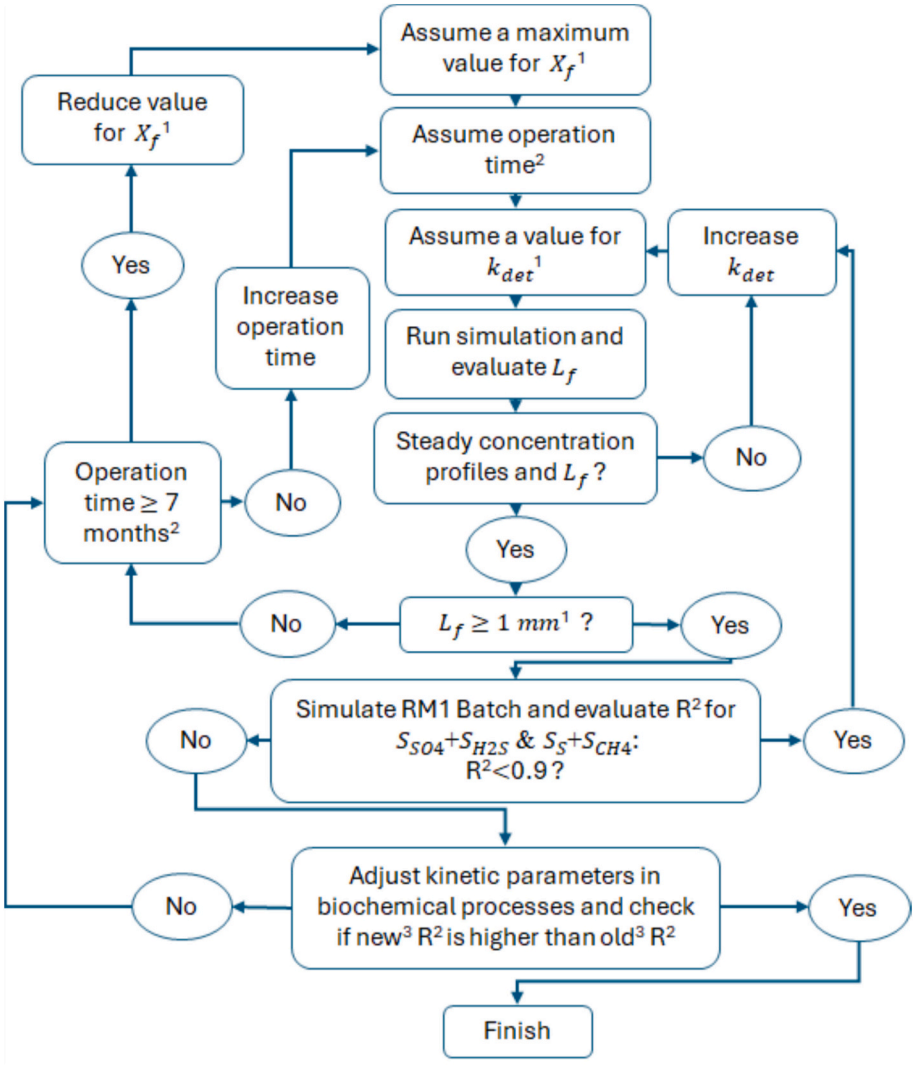

Fig. 1. Manual calibration procedure.1: Values obtained from the literature [62]; 2: Operation time assumed based on the experimental data; 3: New and old are R^2 values from current and previous simulation iterations, respectively.

using a constant feed rate, evaluated as 0.012 ($\frac{m^3}{d}$), which was calculated based on the average HRT of the system. Switching the feed mode from sequential to continuous could affect the ABRM predictions accuracy. Results of the validation process were used to evaluate this prospect.

Calibration was performed manually by adjusting several key unspecified system characteristics (biofilm thickness, biomass density, and detachment rate) and key model process parameters (biochemical and physico-chemical processes) using the approach presented in the literature [27,61]. The calibration process is shown in Fig. 1, where if any adjustment was made the simulation was ran from the beginning point of operation.

Manual calibration of the ABRM progressed depending on an assumed value for X_f not exceeding a maximum limit and the predicted value of L_f reaching a steady state constant value in all four reactors. As no values were provided for X_f and L_f in the cited source of the experimental data, reliable values were chosen based on a published study that experimentally evaluated both variables in a pilot-scale sewer system [62]. Therefore, it is important to highlight that the chosen values for the two aforementioned variables are case specific and depend on the conditions of the biofilm being modelled.

To terminate the calibration processes, the coefficient of determination (R^2) is used twice to assess the quality of predictions provided by the model. First, as show in Fig. 1, the experimental batch study conducted using RM1 is simulated using the ABRM and R^2 (old) is calculated for each of the reported and predicted concentrations of S_{SO4}, S_{H2S}, S_S ($S_{Su} + S_{AA}$), and S_{CH4}. The calibration processes progress, unless any of the evaluated R^2 was found to be <0.9, then the value of k_{det} is adjusted and the simulation is repeated. A minimum value of 0.9 for R^2 was chosen due to the complexity of the model. Second, the kinetic parameters of the biochemical processes are adjusted, and the simulation repeated. The calibration process is terminated after this last step if all evaluated R^2 (new) were higher than 0.9.

Parameters for biochemical and physico-chemical processes obtained from the literature were for systems operated at temperature range between 33 and 35 °C. To be able to use them in the ABRM, their values were changed to fit the temperature used in the experimental data (23 °C). The effect of operating temperature on the various biochemical and physico-chemical processes influencing the anaerobic biofilm is widely recognised [4,63].

Values of the literature sourced parameters were corrected to match the desired temperature using the van't Hof–Arrhenius equation [64,65]:

$$k_{T2} = k_{T1} e^{\theta(T2-T1)} \tag{39}$$

where k_{T2} and k_{T1} are the temperature corrected rate coefficient at temperature $T2$ and the reference rate coefficient at temperature $T1$, $T2$ and $T1$ are operational and reference temperatures ($°C$), and θ is the temperature coefficient. In this model, the coefficients that were considered for temperature dependency were: diffusion coefficients (mass transfer resistance), biokinetics parameters (maximum uptake rates, half saturation rate constants, and inactivation/decay constants), gas transfer coefficients, Henry's gas constants, and acid/base dissociation constants. In the calibration process, adjustments were made on the reference value of the parameter (k_{T1}).

To validate the ABRM, its predictive ability was tested by comparing its calibrated output in two simulations representing two experimental scenarios: the 3 remaining batch studies (RM2, 3, and 4), and the continuous operation experimental data study. The former tested the model's ability in predicting the different biofilms microbial activity, while the latter tested the model's ability in predicting the resultant spatial differences in each microbial biofilm activity. To completely represent the continuous operation of the lab scale system, the simulated operation was switched to a sequential feed with changing HRT. Spearman's rank correlation coefficients were calculated between the experimental concentration data and the ABRM output to assess the predictive capability of the model. Spearman's rank correlation coefficient is used to compare results by evaluating the relationship between two sets of ranked data. Its values range from 1.0, indicating a perfect positive correlation, to −1.0, indicating a perfect negative correlation. A positive correlation signifies that both variables increase or decrease together, while a negative correlation indicates that one variable increases as the other decreases [66]. Spearman's rank correlation coefficient was evaluated using the cited experimental data for the concentrations of S_{SO4}, S_{H2S}, S_{VFAs}, and S_{CH4} during the daily operation of RM2 and 3 and their ABRM predicted counterparts.

2.6.3. Examining spatial variations in the system performance

The continuous operation experimental data (Section 2.6.1) showed a difference in S_{SO4}, S_{H2S}, S_{VFAs}, and S_{CH4} between the consecutive reactors (RM2 and RM3). Indicating a spatial variation in microbial activity in the four reactor's system. The ABRM was used as a tool to obtain a basic understanding of changes in the biofilm microbial structure and the multitude of associated microbial activities that induced this variation.

Simulation results of the operation leading to the establishment of steady anaerobic biofilm was used to examine the microbial structure, biofilm characteristics, pH levels, and production levels of the targeted group of malodorous VSCs and VFAs in the four developed biofilms, in order to identify any resultant differences between them due to their placement in the lab scale system. To examine the microbial species distribution and activity in each of the developed biofilms, simulation results for the microbial species distribution inside each biofilm were clustered as five functional groups: FG1; fermentative (X_{su}, X_{AA}, and X_{fa}), FG2; Ac and H_2 producers (X_{C4} and X_{Pro}), FG3; CH_4 producers (X_{Ac} and X_{H2}), FG4; SO_4^{-2} reducers ($X_{SRB,Pro}$, $X_{SRB,Ac}$, and $X_{SRB,H2}$), and FG5; inerts (X_I). The relative abundance of each group (RA_i) in the biofilm reactor predicted operation is then evaluated for each developed biofilm using Eq. (40):

$$RA_i = \frac{\sum_{j=1}^{n} X_j}{\sum_{k=1}^{m} X_k} \tag{40}$$

where RA_i is the relative abundance of the functional group i (i = FG1, 2, 3, 4, and 5) in the developed reactor's biofilm, n is the total number of microbial species in each functional group i in all layer segments inside the reactor's biofilm, and m is total number of microbial species in all layer segments (Section 2.7) inside the reactor's biofilm.

2.6.4. Estimating malodorous VSCs and VFAs emissions

To provide a complete picture, and to fully explore the ABRM ability, the dynamic levels of the targeted group of malodorous VSCs and VFA emissions were estimated for the lab scale system. To perform this task, a simulation was performed in a modified lab scale system. The modification included adding an open reactor (RM5) that receives the resulting flow from the original 4. RM5 has no biological activity and includes a headspace that allows for gaseous emissions of the resulting targeted malodorous VSCs and VFAs to the atmosphere. The headspace volume was assumed to be 20 % of the liquid volume [67]. Fig. 2 shows a schematic of the emissions simulation system.

For this simulation, the system of reactors was assumed to be fed with the same screened and settled wastewater, as reported in the published work used in the calibration and validation of the anaerobic reactor model [32]. Additionally, to investigate the effect of dynamically changing HRT, emissions were estimated for the lab scale system during the monitoring period that included 10 pumping events, which was used to validate the ABRM continuous operation predictions. In this simulation, gas flow is assumed to circulate inside the headspace of RM5, influent VSCs and VFAs free gas is introduced at a rate equal to the gas flowrate produced by the system (Eq. (37)).

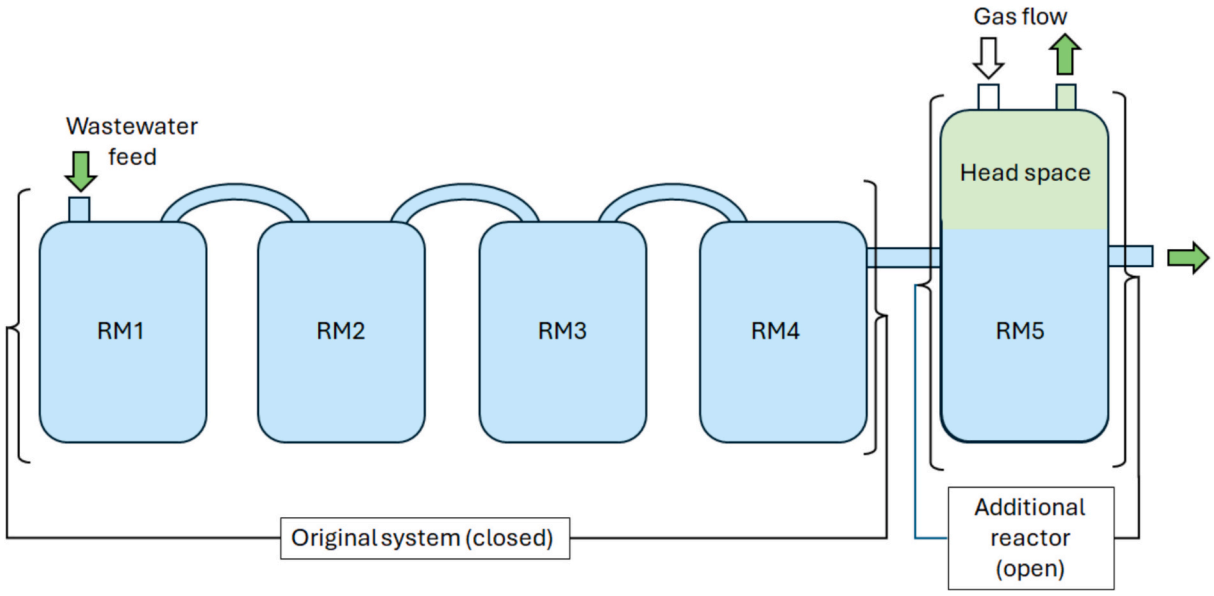

Fig. 2. The modified 5 reactor emissions simulation system.

As a measure of the system potential to produce the targeted group of malodorous VSCs and VFAs, daily emission levels of H_2S, MT, VFAs, and CH_4 were evaluated as follows (Eq. (41)):

$$q_{i,G}(t) = q_G(t)S_{i,g}(t) \tag{41}$$

where $q_{i,G}$ is the daily emission level of compound i $\left(\frac{Mass}{d}\right)$.

2.7. Model simulation

Simulations were performed for the ABRM by simultaneously solving the system's biofilm, liquid and gas phase equations. Mathematically, the partial differential equations for the biofilm phase were transformed to ordinary differential equations through discretization in the perpendicular direction (z in the model equations) of the biofilm. The biofilm was segmented into 8 sections and the variables in each segment were evaluated using the finite difference method and the relevant boundary conditions. The resulting ordinary differential equations in time were solved (MATLAB® 2021, Ode 15 s) simultaneously with the liquid and gas phases to provide predicted values of the modelled variables with time. Initial values of the parameters in the ABRM biochemical and physico-chemical processes were obtained follows:

1. Biochemical processes:
   a. Anaerobic digestion: ADM1 within the BMS2 framework: [44].
   b. SO_4^{-2} reduction and H_2S inhibition: [55,68–71]
2. Physico-chemical processes:
   a. Acid/base: ADM1 within the BMS2 framework: [44]
   b. Biofilm-liquid transport and biofilm diffusion: [72,73].
   c. Liquid-gas transport: [44,65,74].
   d. Temperature dependency: [65,70]

3. Results and discussion

3.1. ABRM calibration

The accompanying information with the experiential data used in this work did not provide any categorization for the dissolved degradable COD found in the feed of the lab scale reactor system. Therefore, following the Activated Sludge Model No. 2d (ASM2d) to ADM1 interface [75], it was assumed that the dissolved degradable COD concentration can be estimated as $S_{AA} + S_{Su}$, with S_{Fa} being considered negligible. As for the remaining unknown dissolved components in the feed, values specified in BSM2 were used [44]. The initial values for the volume fractions of the microbial species inside the biofilms were assumed identical, and the initial values for the biofilm thicknesses were assumed to be 1 mm for all reactors.

A stable steady state was assumed to be reached depending on the biofilm thickness and production profiles inside the reactors (at constant feed flow rate). The system reached steady state after 180 days of simulated operation. For the initial conditions in the batch tests (species distribution in the biofilm, biofilm thickness, and biomass density), the resulting lab system conditions after the 180-day simulated operation was used. Fig. 3A1 and B1 shows the time course concentration data for the experimental batch test for RM1 and the ABRM output after manual calibration.

The ABRM provided largely good predictions for the simulated species in RM1 batch tests. Values for R^2 for the predicted concentrations were 0.973, 0.961, 0.916, and 0.931 for S_{SO4}, S_{H2S}, S_S ($S_{Su} + S_{AA}$), and S_{CH4}, respectively. The calibration processes also estimated the value of X_f to be 35 ($\frac{kg\ COD}{m^3}$). While this value was not provided in the cited sources of experimental data, it was found to be within reported values for anaerobic biofilms in the literature [62]. The estimated value for k_{det} in RM1 biofilm was 8.44 ($\frac{1}{d.m}$). However, using this value in the remaining reactors caused the model to fail in predicting the experimental batch tests results. Therefore, this value was changed for each one of the remaining three biofilms to 9.28, 9.70, and 10.55 ($\frac{1}{d.m}$) for RM2, RM3, and RM4, respectively. It must be added that the obtained values for X_f and k_{det} resulted from the prescribed manual calibration approach, as discussed in Section 2.6.2, warranted by the lack of their mention in the cited source of experimental data. While this approach was followed in the literature with great success [76,77], the obtained values for the two parameters remain systems specific.

Table 2 lists the estimated values for the biochemical processes parameters resulting from the calibration process. The remaining parameters maintained their values specified in Section 2.5. As seen in Table 2, estimated parameters for the biochemical processes associated with SRB were within values listed in the literature for processes utilizing the same inhibition functions used in this work. As a multitude of formulations exist in the literature for SRB inhibition functions with no clear justification given for the usage of a specific function, mainly due to their empirical nature [68]. Among the three substrates utilized by SRB,

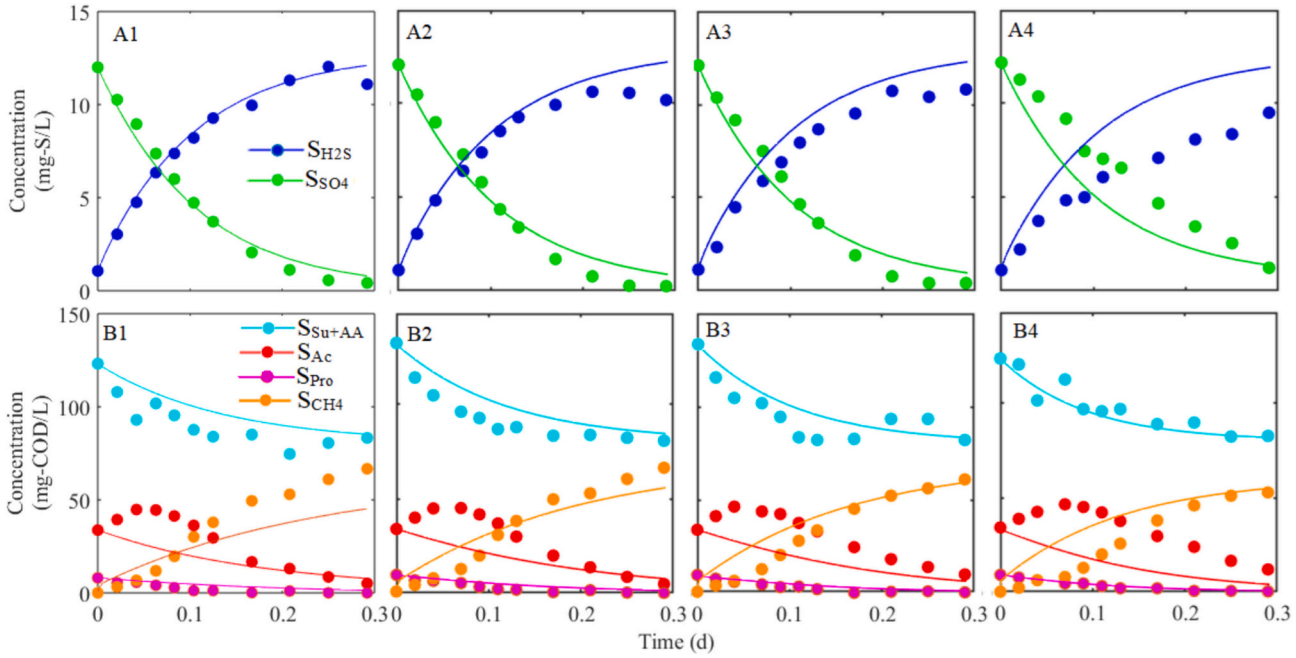

Fig. 3. Time course concentration data for the experimental batch tests and the ABRM; A1 to 4): H_2S and SO_4^{-2} in RM1 to RM4; B1 to 4): COD in RM1 to RM4 (S_S=S_{Su}+S_{AA}); Lines represent the biofilm model output after manual calibration and dots represent experimental data [32].

H_2 had the highest uptake rate, this could be attributed to the high C/S ratio of the feed wastewater (≅13.3) favouring the usage of H_2 in SRB [78]. For the biochemical processes associated with methanogenesis, resulting value were on the higher side of those in reported literature. This could be attributed to the type of wastewater used in the feed of the experimental system [75,79].

Overall, the ABRM was largely successful in predicting the experimental profiles for the sulphur species (Fig. 3A2, A3, and A4), and VFAs and CH_4 (Fig. 3B2, B3, and B4) in the batch tests for RM2, 3, and 4. Both the experimental data and model predictions demonstrated the simultaneous SO_4^{-2} reduction and CH_4 production in the reactors. The results suggested that the developed ABRM was able to replicate the experimental data reasonably well, which suggested that the developed model could correctly describe CH_4 production and SO_4^{-2} reduction in the batch studies, thus validating the ABRM developed in this work.

3.2. Simulation of the continuous operation data

Fig. 4 shows the ABRM predicted vs measured concentrations during the 10 pumping events within the daily monitoring period of the lab scale system. To match the conditions of the experimental data, the simulated operation of the lab scale system was switched to a sequential daily wastewater feeding mode. Each day, 7.6×10^{-4} (m^3) of wastewater was pumped into the system multiple times at the following time intervals: 0, 6, 7, 8, 8.5, 9, 9.5, 10, 12, 15, 18, and 22 h. This data was obtained by examining the results figures shown in the cited paper.

The ABRM was able to reproduce the trends in S_{SO4}/S_{H2S} and S_{VFAs}/S_{CH4} reasonably well in RM2 and 3 (Figs. B1 and B2, and C1 and C2). Indeed, the Spearman's rank correlation coefficients for the eight measured concentrations and their predicted counterparts were 1, 1, 0.922, and 0.929 for S_{SO4}, S_{H2S}, S_{VFAs}, and S_{CH4}, respectively, indicating a good and reasonable fit. Therefore, ABRM was able to successfully predict the spatial and temporal variations found in the experimental system data between RM2 and 3. Theses spatial and temporal variations were also shown to be found in the remaining reactors, as shown in Figs. A1 and A2, and D1 and D2 for RM1 and RM 4, respectively. The predicted data also showed the variation in pH levels in all the lab scale reactors, where spatial and temporal variations in microbial activity were reflected in the changing levels of pH in the reactors. Spatial variation in microbial biofilms activity was reported in the literature for anaerobic sewer biofilms [35].

Despite the Spearman's rank correlation coefficients values showed that the ABRM represented the trend of the experimental data reasonably well, some discrepancies were found between the empirical and predicted concentrations. These differences could be attributed to the fact that the model assumed ideal mixing conditions in the reactors. These discrepancies could possibly be reduced or limited by accurately detecting the mixing regime of the lab scale system and using the ABRM in the resulting CRN configuration.

The examination of the change in predicted concentrations inside each reactor shows that the ABRM was also successful in reflecting the changes in activity brought about by the sequential change in HRT. As shown in Fig. 4, a reduction in biofilm activity is shown as HRT is decreased, with rising values of S_{SO4} and S_{VFAs} and descending values of S_{H2S} and S_{CH4}. This becomes clear when observing the increased levels of S_{H2S} and S_{CH4}, as HRT is increased. Furthermore, the increase and decrease in activity was mirrored by the predicted pH trends in all the reactors. An increase in methanogenic activity will result in an increase in pH, and vice versa. The observation is supported by the literature, where longer HRTs promotes the biological activity in sewer networks [80].

As shown in Fig. 4 A1, B1, C1, and D1, the ABRM was able to provide an estimate of the level of produced MT in all the reactors, where its levels were also related to changes in HRT. In this model, MT and H_2S are assumed to be released as a result of sulphur containing AAs, and their production rate from this process is calculated stoichiometrically relative to the processes of AAs uptake in the biofilm, which was also affected by the changing HRT. However, it must be added that the ABRM predicted levels of MT production are directly related to the assumed fraction of S_{AA} in the dissolved degradable COD concentration in the wastewater feed, which was 50 %. Therefore, the predicted levels of MT production come with some uncertainty that stems from the validity of the assumed fraction of S_{AA} in the feed wastewater.

Overall, the ARBM ability to successfully predicting the spatial variation between the lab scale system reactors performances and in predicting the change in performance for each one of them under

Table 2
Estimated values for the biochemical processes' parameters.

Process	Parameter	Values[a]		Reference
		Literature	Calibrated	
Uptake of S_{Su}	$k_{m,Su}$ $(\frac{1}{d})$	30	45	[44,69]
	$K_{S,Su}$ $(\frac{kg\ COD}{m^3})$	0.5	0.4	
Uptake of S_{aa}	$k_{m,AA}$ $(\frac{1}{d})$	50	65	
	$K_{S,AA}$ $(\frac{kg\ COD}{m^3})$	0.3	0.28	
Uptake of S_{Fa}	$k_{m,Fa}$ $(\frac{1}{d})$	6	9	
	$K_{S,Fa}$ $(\frac{kg\ COD}{m^3})$	0.4	0.4	
Uptake of S_{Va}&S_{Bu}	$k_{m,C4}$ $(\frac{1}{d})$	20	30	
	$K_{S,C4}$ $(\frac{kg\ COD}{m^3})$	0.2	0.17	
Uptake of S_{Pro}	$k_{m,Pro}$ $(\frac{1}{d})$	13	28	
	$K_{S,Pro}$ $(\frac{kg\ COD}{m^3})$	0.1	0.4	
Uptake of S_{Ac}	$k_{m,Ac}$ $(\frac{1}{d})$	8–13	12	
	$K_{S,Ac}$ $(\frac{kg\ COD}{m^3})$	0.15	0.15	
Uptake of S_{H2}	$k_{m,H2}$ $(\frac{1}{d})$	35–40	42	
	$K_{S,H2}$ $(\frac{kg\ COD}{m^3})$	7×10^{-6}	6.6×10^{-6}	
Free H_2S inhibition to S_{Ac} and S_{H2}uptake in ADM1	$K_{I,H2S,\rho 11\ and\ \rho 12}$ (M)	$4.4–8.9 \times 10^{-3}$	8×10^{-3}	[71,68]
SRB with S_{Pro}	$k_{m,SRB,Pro}$ $(\frac{1}{d})$	12.6–42	29.6	[55,68,69,70]
	$K_{S,SRB,Pro}$ $(\frac{kg\ COD}{m^3})$	0.1–0.3	0.1	
	$K_{S,SO4,Pro}$ (M)	7.7×10^{-5} - 2.3×10^{-4}	1.06×10^{-4}	
SRB with S_{Ac}	$k_{m,SRB,Ac}$ $(\frac{1}{d})$	7.1–17	9	
	$K_{S,SRB,Ac}$ $(\frac{kg\ COD}{m^3})$	0.024–0.29	0.019	
	$K_{S,SO4,Ac}$ (M)	1×10^{-4} - 6×10^{-4}	1×10^{-4}	
SRB with S_{H2}	$k_{m,SRB,H2}$ $(\frac{1}{d})$	12–45	40	
	$K_{S,SRB,Ac}$ $(\frac{kg\ COD}{m^3})$	2.5×10^{-5} - 1×10^{-4}	8×10^{-5}	
	$K_{S,SO4,Ac}$ (M)	2.8×10^{-5} - 2×10^{-4}	2.8×10^{-5}	

[a] Values at the reference temperature of 35 °C in the temperature correction equation.

varying HRT, validates its predictive ability under the conditions of this study. Furthermore, the introduced simplification of opting for a constant feed rate in the initial phase of model simulations did not severely affect the quality and usefulness of those predictions. The resulting spatial variation of biological activity is further discussed in Section 3.3.

3.3. Examining spatial variations in the system performance

To investigate the resulting spatial variation in the experimental biofilm, steady state values resulting from the system simulation under constant HRT were analysed. Fig. 5 shows the ABRM predicted biofilm thickness, pH, and production levels of the targeted group of malodorous VSCs and VFAs in each reactor during its simulated operation at 23 °C.

The increased level of pH in the reactors indicate that biological methane production continued sequentially in the four reactors (Fig. 5A). However, the reduction in biofilm thickness (Fig. 5B) revealed that this was accompanied with reduced biological growth. The drop in biofilm thickness resulted in estimated biomass levels of 0.0897, 0.0728, 0.0592, and 0.0465 $(\frac{kg\ COD}{m^2})$. This reduction in biomass levels caused a decrease in biological activity, as it can be seen by the concentration profiles of the sulphur and carbon species in the reactors (Fig. 5C and D). S_{SO4} dropped and S_{H2S} increased by 5.9, 3.6, 2.1, and 1.2 $(\frac{mg-S}{L})$, in RM1, 2, 3, and 4, respectively, which showed a reduction in substrate uptake levels by SRB. The same observation could be made for methanogens, as the combined level of S_{Su}, S_{AA}, and S_{Fa} dropped by 0.04, 0.03, 0.02, 0.014 $(\frac{kg\ COD}{m^3})$, with S_{CH4} increase by 0.024, 0.022, 0.02, 0.017 $(\frac{kg\ COD}{m^3})$, in RM1, 2, 3, and 4, respectively. Regarding the level of MT production, the ABRM assumes that it is released as a result to the uptake of sulphur containing AA, so its production rate in the four reactors followed the level of S_{Su}, S_{AA}, and S_{Fa} uptake. This drop in biomass levels and reduced biological activity can be attributed to the reduction in substrate levels in the reactors. As fresh feed is only introduced to RM1, with each of following reactors receiving the effluent from reactor before it. This observation was reported in the literature for sewer biofilm, as anaerobic biofilms developed upstream showed higher levels of microbial growth and substrate utilization compared to those found downstream [33]. Overall, from the previous discussion, the ABRM was successful in quantifying the spatial variation in the anaerobic biofilm activity between the four reactors.

Fig. 6 shows the predicted relative abundance (Eq. (37)) of the 5 functional groups inside the developed anaerobic biofilms (A) and predicted volume fraction of the 5 functional groups inside the 8 segments of developed anaerobic biofilms in each reactor (B, C, D, and E).

The predicted relative abundance for SRB was significantly lower than that for methanogens in all reactors, indicating that under the conditions of this simulation, methanogens outcompeted SRB in the anaerobic biofilm (Fig. 6A). These predictions are well supported by the literature, and they came as a result to the nature of substrates required by the two functional groups. While both microbial groups utilize the same organic substrates in the anaerobic biofilm as electron donors (Acetate and Hydrogen), SRB growth also depends on the levels of SO_4^{-2} inside the biofilm. SO_4^{-2} is not produced inside the biofilm and requires transport from the liquid phase, and its levels is affected by the rate of mass transfer which is dictated by the concentration gradient between the liquid and biofilm phases [31,32,35]. In contrast, the required substrates for methanogens are mainly produced in situ and do not require transport from the liquid phase to the biofilm [32].

Fig. 7 shows the concentration profiles for S_{SO4}, S_{H2s}, and S_{MT} in the anaerobic biofilms inside each reactor. Inspecting the ABRM predictions for the SO_4^{-2} concentrations inside the layers of the biofilm supports the previous observations. As it can be seen in Fig. 6A, the predicted concentrations of S_{SO4} in the outer layer (L1) were 4.5, 3.5, 2.6, and 1.9 $(\frac{mg-S}{L})$, in RM1, 2, 3, and 4, respectively. Comparing these values to the liquid phase concentrations of S_{SO4} (Fig. 4C), will reveal a successive reduction in SO_4^{-2} concentration gradients, which were 5.1, 2, 0.8, and 0.3 $(\frac{mg-S}{L})$, in RM1, 2, 3, and 4, respectively. This indicated a decrease in the driving force for mass transfer from one reactor to another.

Distinct diversity distribution characteristics will result in the microbial biofilm as a result of the nature of substrates required by SRB and methanogens. The association between SRB and SO_4^{-2} levels will result in the development of higher volume fractions of SRB near the outer layers of the biofilm, where higher concentrations of SO_4^{-2} can be found (Fig. 7A). On the other hand, methanogens will have higher volume fractions in the inner layers [21,37]. This aspect was also predicted by the ABRM as shown in Fig. 6B, C, D, and E in layers 1 to 4 in RM1 and 2, and from layers 1 to 5 in RM3 and 5.

Finally, another aspect of SRB and methanogens competition predicted by the model are the differences in their susceptibility to free H_2S inhibition. Higher levels of H_2S were predicted in the inner layers,

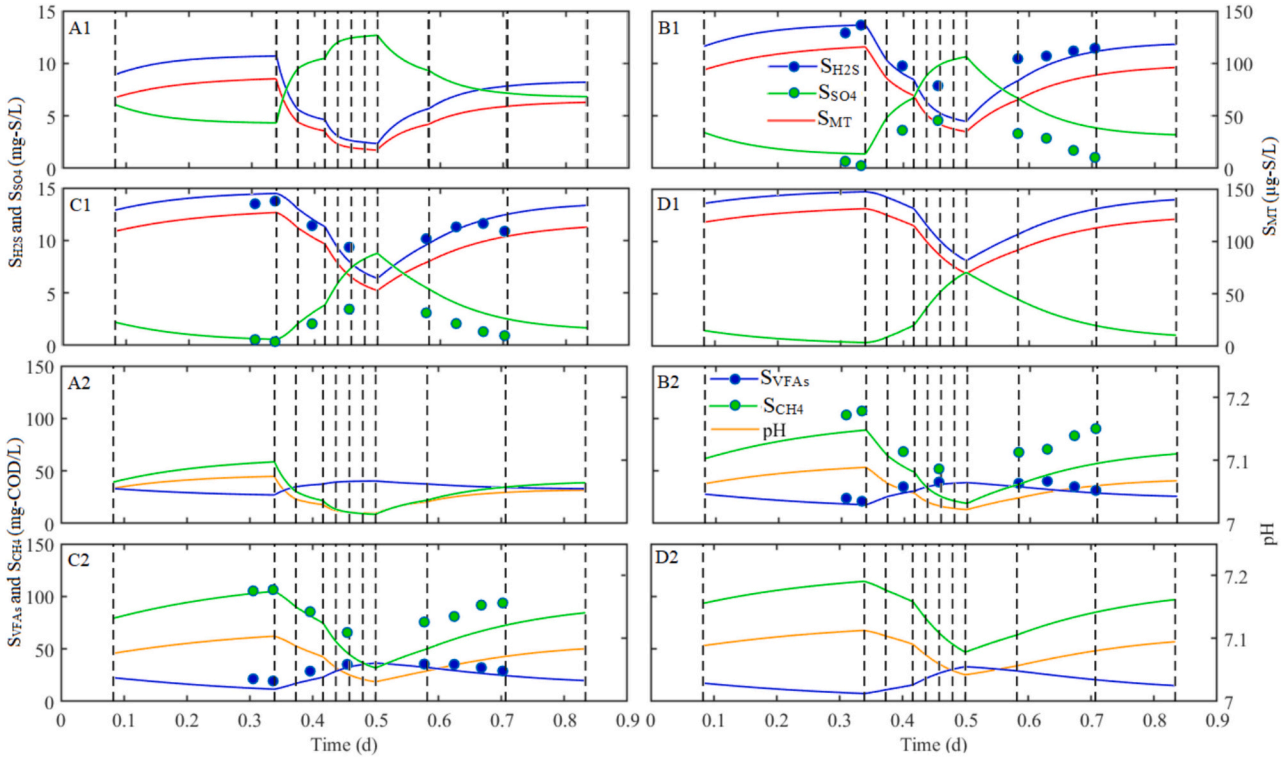

Fig. 4. The ABRM predicted (lines) vs measured (dots) concentrations during the 10 pumping events within a day of operation for A) RM1, B) RM2, C) RM3, and D) RM4, where 1) S_{SO4}, S_{H2S}, and S_{MT} and 2) pH, S_{VFAs}, and S_{CH4}. Vertical lines indicate a change in hydraulic retention time in the system.

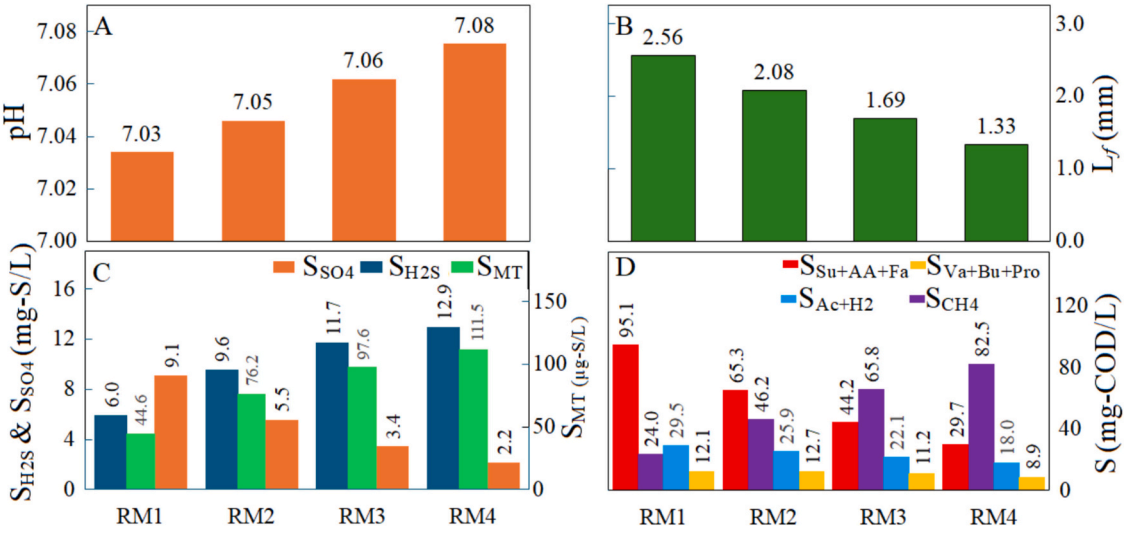

Fig. 5. Predicted output BFRM of each one of the reactors after 180 days of simulated operation; A) pH, B) L_f, C) S_{SO4}, S_{MT}, and S_{H2S}, and D) COD fractions.

reaching levels of 11.6, 12.79, 13.532, and 13.96 ($\frac{mg-S}{L}$) in the biofilms of RM1, 2, 3, and 4, respectively (Fig. 7B). Compared to SRB, methanogens are more susceptible to H_2S inhibition, indicated by their lower inhibition constant [69,71]. Therefore, as shown in Fig. 6B, the volume fractions of methanogens dropped in favour of SRB from layer 5 to layer 8 (RM1 and 2), and from layer 6 to layer 8 (RM3 and 5). However, the gains in volume fraction achieved by SRB diminished as S_{H2S} in the inner layers increased to levels that increases their susceptibility to free H_2S inhibition (Fig. 6E vs Fig. 6B, C, and D).

Overall, the ABRM was able to provide a level of basic understanding of the changes in the biofilm microbial structure and the multitude of associated microbial activities that led to the spatial variations reported in the experimental data. Successfully depicting the ensuing spatial variations in the anaerobic methanogenic biofilm's species distribution, abundance, growth, activity, substrate uptake, and production levels of the targeted group of malodorous VSCs and VOCs in all the system reactors.

3.4. Estimating malodorous VSCs and VFAs emissions

By introducing a fifth reactor (RM5) at the receiving end of the lab scale system, the level of produced malodorous VSCs and VFAs emissions could dynamically be estimated without disturbing the operation of the first four. Fig. 8 shows the predicted output of RM5 during the 10

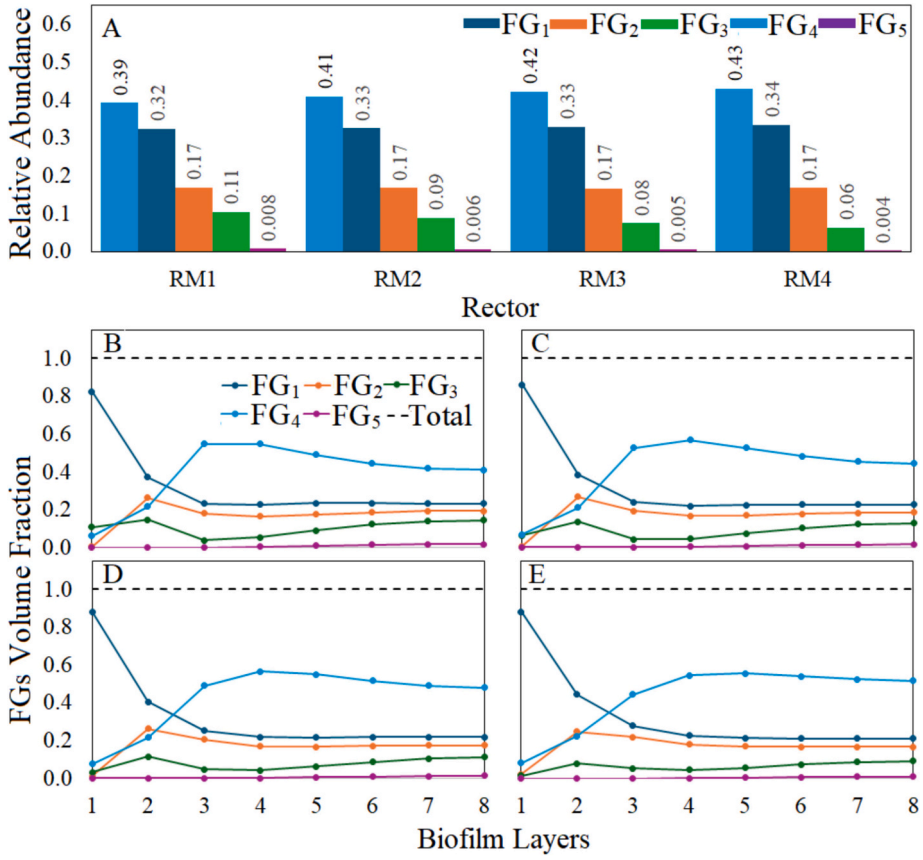

Fig. 6. A) Predicted distribution of the 5 functional groups within each developed biofilm, and predicted volume fraction of the 5 functional groups inside the 8 segments of the developed anaerobic biofilms in B) RM1, C) RM2, D RM3, and E) RM4.

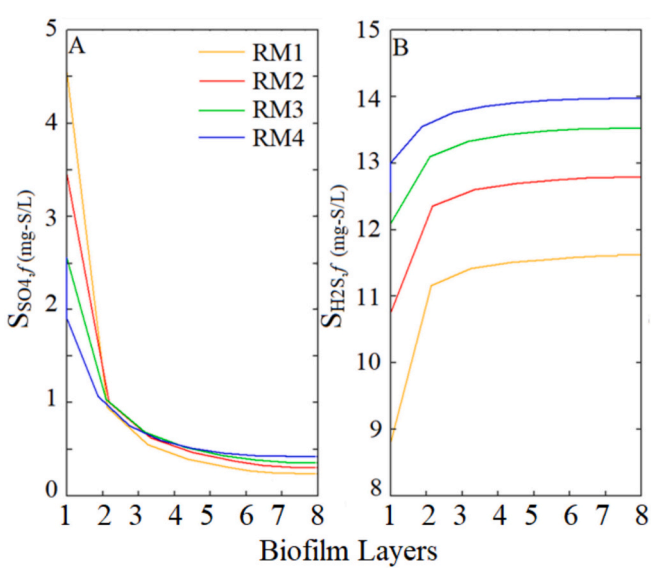

Fig. 7. Concentration profiles for A) $S_{SO4,f}$ and B) $S_{H2S,f}$ in the anaerobic biofilms of the four reactors.

pumping events within a day of operation.

The total gas flow rate is evaluated in the ABRM by calculating the individual gas transport rates for all gaseous species in the reactor (Eq. (17)). Therefore, the resulting gas flow is dependent on the level of those transport rates, and consequently the level of transported compound in the liquid phase. Additionally, gas flow rate is largely dependent on two major contributors, CH_4 and CO_2. The gas flow rate of the targeted group of malodorous VSCs and VFAs initially increased with reduced HRT (increased flow rate) as shown in Fig. 8A. Lower HRTs will increase the level of a compound replenishment inside the reactor liquid phase, rapidly increasing its concentration, and maintaining a larger gradient for the liquid-gas transport process (Fig. 8E and F).

This can be seen by comparing the feed cycles in periods 1 and 3 to periods 2 and 4 in Fig. 8B, C, and D. However, this behaviour depends on the concentration of the compound in the incoming feed. As seen in Fig. 4D1 and D2, the reduced HRT in the system resulted in a decline in the microbial activity of the anaerobic biofilms, reducing the level of H_2S, MT, and CH_4 in the effluent of RM4 and the feed to RM5. In this case, the reduced HRT will have a wash-out effect in the content of RM5 i.e. rapidly introducing a feed that has a lower concentration than what is inside the reactor (Fig. 8E and F). This can be seen in the feeding cycles in time period 5, where the high flow rate of low concentration feed is maintained. This observation is supported by examining the gas transport rates of VFAs (Fig. 8D) in the same period (5), where their transport rate increased mainly due to their higher concentration in the incoming feed, which resulted from the reduced anaerobic biofilm activity (Fig. 4D). The effect of influent dynamics on the level of malodours emissions is documented in the literature [12]. And as it can be seen from the previous discussion, these effects are partially associated with the changes taking place upstream, as changes in RM1 to 4 were reflected as changes in emissions rate from RM5.

Another important aspect that maintained increased the gas transport of VFAs in time period 5 was the drop in pH, which was attributed to the increased removal of CO_2 in the previous time periods (Fig. 8C) [80]. This aspect is clarified by examining the levels of acid/base forming compounds in RM5, which is shown in Fig. 8H, I, and J. For acid/base pair forming compounds, liquid gas transfer is achieved by the free and protonated form of the compound. Lower pH values increased

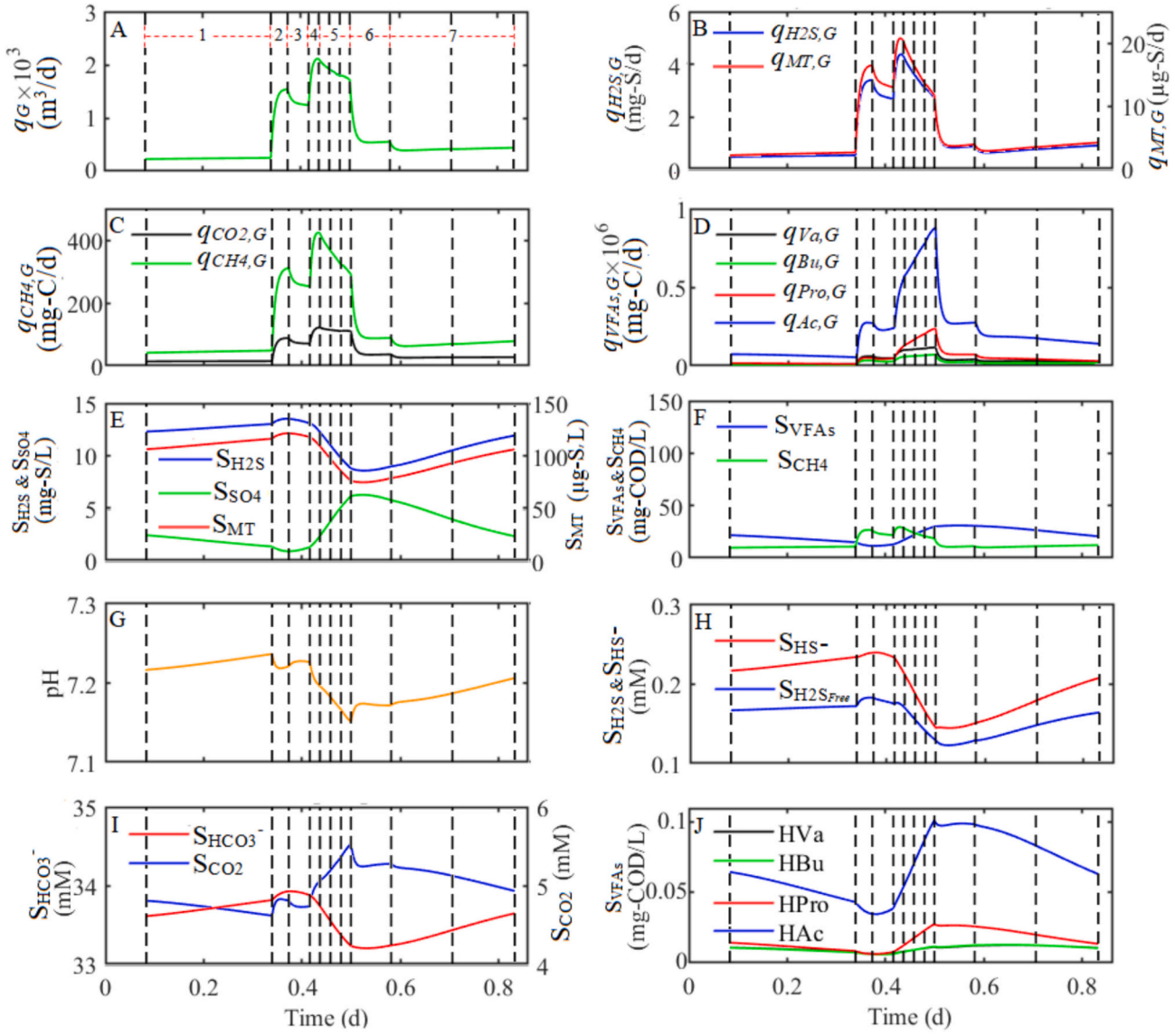

Fig. 8. Predicted output of RM5 during the 10 pumping events within a day of operation: A) q_G, B) $q_{H2S,G}$ and $q_{MT,G}$, C) $q_{CH4,G}$ and $q_{CO2,G}$, D) $q_{Ac,G}$, $q_{Pro,G}$, $q_{Bu,G}$, and $q_{Va,G}$, E) S_{H2s}, S_{MT}, and S_{SO4}, F) S_{VFAs}, and S_{CH4}, G) pH, H) S_{HS^-} and $S_{H2S^{Free}}$, I) S_{HCO3^-} and S_{CO2}, and J) Free S_{VFAs}.

the level of free VFAs in RM5 (Fig. 8G and J), therefore increasing their gas transfer rate. The drop of pH in RM5 also affected the gas transfer rate of H_2S and CO_2, where their free form increased in response to the decrease in pH (Fig. 8H and I), resulting in a slower decline in their gas transfer rates, compared to the other compounds (Fig. 8B and C); a drop by 37 % vs 42 % for H_2S and MT, respectively, and 8 % vs 30 % for CO_2 and CH_4, respectively. In time periods 6 and 7, the decline in gas transfer rates and gas flow rate continued as levels of one of the major contributors to the gas flow rate (CH_4) in RM5 dropped even lower (Fig. 8F).

Overall, the ABRM was able to provide dynamic estimates for the levels of the targeted malodorous VSCs and VFAs emissions in the system under varying operational conditions (multiple HRTs). Highlighting the effect of key factors (such as pH) on their production.

The proposed model discussed herein was able to predict the production of a group of malodorous VSCs and VFAs resulting from anaerobic microbial biofilms. Providing the ability to dynamically predict the ensuing effects from changes in the biofilm surrounding conditions on its activity. Under the conditions of this study, the model showed that changes in HRT and levels of substrate in the liquid phase at the biofilm's vicinity have a paramount effect on the biofilm's activity. These changes in operational conditions were key in dictating the microbial community structure in the studied biofilms. Moreover, their effect was also important in the resulting level of malodorous emissions of the targeted group of compounds.

The usage of state-of-the-art framework, and the possibility of its application within a CRN framework makes the ABRM a valuable tool in plant-wide integrated approach studies. Not only for the purpose of malodorous emissions estimation, but also for day-to-day operation assessment, optimization, and monitoring for units that employ biofilms in their operation, like anaerobic membrane bioreactors. Furthermore, the ABRM current structure allows for the inclusion of the effect of changing other operational parameters such as organic loading, C/S ratio, the presence of suspended biomass, and temperature. Which can be included with proper experimentation.

4. Conclusions

A mathematical model that can dynamically simulate the production and emission of a group of malodorous VSCs and VFAs resulting from an anaerobic, methanogenic, sulphate reducing microbial biofilms was developed. The biofilm was modelled using a multispecies approach, and the well-established ADM1 framework was used to represent the

microbial activity, after amending it with additional biochemical and physico-chemical processes to accurately represent the interactions found in anaerobic methanogenic sulphate reducing biofilms. The model was formulated as an integrated anaerobic biofilm reactor model that provides a combined output based on the process taking place in the biofilm, liquid, and gas phases, in order to facilitate its application as a part of a chemical reactor network that could represent different hydrodynamic mixing conditions. Published experimental data for a lab scale, anaerobic biofilm containing system, fed with real wastewater was used to calibrate and validate the ABRM. The model provided a quantitative representation for spatial variations in the anaerobic biofilm's microbial species distribution and abundance, growth and activity, substrate uptake, and the levels of the targeted malodorous VSCs and VFAs production and emissions in response to changes in prevailing operational conditions. The model was able to express the interactions between SRB and methanogens in the biofilm, delineating the effect of substrate competition and H_2S inhibition on the diversity distribution characteristics inside the biofilm. Finally, the ABRM was used to provide dynamic estimates for the levels of production for targeted malodorous VSCs and VFAs emissions in the system under varying operational conditions.

Abbreviations

AA:	Amino acids
ABRM:	Anaerobic Biofilm Reactor Model
Ac:	Acetate
ADM1:	Anaerobic Digestion Model No. 1
BSM2:	Benchmark Simulation Model no. 2.
ASM2d:	The Activated Sludge Model No. 2d
Bu:	Butyrate.
CH_4:	Methane.
COD:	Chemical oxygen demand.
CO_2:	Carbon dioxide.
CRN:	Chemical Reactor Network.
Fa:	Long-chain fatty acids.
H_2:	Hydrogen.
HRT:	Hydraulic retention time.
HS^-:	Bisulfide.
H_2S:	Hydrogen sulphide.
IWA:	International Water Association.
MT:	Mercaptans.
ODE:	Ordinary differential equation.
Pro:	propanoate.
SO_4^{2}:	Sulphate.
SRB:	Sulphate-reducing bacteria.
Va:	Valerate.
VFAs:	Volatile fatty acids.
VOCs:	Volatile organic carbon compounds.
VSCs:	Volatile sulphurous compounds.
WATS:	Aerobic/anaerobic Transformations in Sewers.
WWTPs:	Wastewater treatment plants.

CRediT authorship contribution statement

Malek G. Hajaya: Writing – review & editing, Writing – original draft, Visualization, Validation, Software, Methodology, Formal analysis, Data curation. **Rawan N. AlKaraki:** Data curation. **Nataliia Kurnikova:** Resources. **Sergio Bordel:** Resources, Funding acquisition. **Raúl Muñoz:** Writing – review & editing, Supervision, Project administration, Funding acquisition, Conceptualization.

Declaration of competing interest

The authors declare that they have no known competing financial interests or personal relationships that could have appeared to influence the work reported in this paper.

Acknowledgments

The Spanish Research Agency and the European Eramus+ KA programmes are gratefully acknowledged for the financial support (PLEC2021-0079439).

Data availability

Data will be made available on request.

References

[1] E.R. Bruce, L.M. Perry, B.E. Rittmann, P.L. McCarty, Environmental Biotechnology: Principles and Applications, McGraw-Hill, New York, NY, 2001.
[2] H. Huang, C. Peng, P. Peng, Y. Lin, X. Zhang, H. Ren, Towards the biofilm characterization and regulation in biological wastewater treatment, Appl. Microbiol. Biotechnol. 103 (2019), https://doi.org/10.1007/s00253-018-9511-6.
[3] U. Wiesmann, I.S. Choi, E.M. Dombrowski, Fundamentals of Biological Wastewater Treatment, 2006, https://doi.org/10.1002/9783527609604.
[4] Z. Lewandowski, J.P. Boltz, Biofilms in water and wastewater treatment, in: Treatise on Water Science, 2011, https://doi.org/10.1016/B978-0-444-53199-5.00095-6.
[5] G. O'Toole, H.B. Kaplan, R. Kolter, Biofilm formation as microbial development, Annu. Rev. Microbiol. 54 (2000), https://doi.org/10.1146/annurev.micro.54.1.49.
[6] T.A. Else, C.R. Pantle, P.S. Amy, Boundaries for biofilm formation: humidity and temperature, Appl. Environ. Microbiol. 69 (2003), https://doi.org/10.1128/AEM.69.8.5006-5010.2003.
[7] V. Vishwakarma, Impact of environmental biofilms: industrial components and its remediation, J. Basic Microbiol. 60 (2020), https://doi.org/10.1002/jobm.201900569.
[8] J. Wingender, H.C. Flemming, Biofilms in drinking water and their role as reservoir for pathogens, Int. J. Hyg. Environ. Health 214 (2011), https://doi.org/10.1016/j.ijheh.2011.05.009.
[9] D. Van Der Kooij, J.S. Vrouwenvelder, H.R. Veenendaal, Elucidation and control of biofilm formation processes in water treatment and distribution using the unified biofilm approach, Water Sci. Technol. (2003), https://doi.org/10.2166/wst.2003.0287.
[10] M. Toledo, R. Muñoz, Optimization of activated sludge recycling and oxidized ammonium recycling as odour control strategies in wastewater treatment plants, J. Water Process Eng. 47 (2022), https://doi.org/10.1016/j.jwpe.2022.102655.
[11] P. Lewkowska, B. Cieślik, T. Dymerski, P. Konieczka, J. Namieśnik, Characteristics of odors emitted from municipal wastewater treatment plant and methods for their identification and deodorization techniques, Environ. Res. 151 (2016), https://doi.org/10.1016/j.envres.2016.08.030.
[12] F. Forouzanmehr, Q.H. Le, K. Solon, V. Maisonnave, O. Daniel, P. Buffiere, S. Gillot, E.I.P. Volcke, Plant-wide investigation of sulfur flows in a water resource recovery facility (WRRF), Sci. Total Environ. 801 (2021), https://doi.org/10.1016/j.scitotenv.2021.149530.
[13] E. Alinezhad, M. Haghighi, F. Rahmani, H. Keshizadeh, M. Abdi, K. Naddafi, Technical and economic investigation of chemical scrubber and bio-filtration in removal of H2S and NH3 from wastewater treatment plant, J. Environ. Manage. 241 (2019), https://doi.org/10.1016/j.jenvman.2019.04.003.
[14] U. Bazemo, E. Gardner, A. Romero, H. Hauduc, A. Al-Omari, I. Takacs, S. Murthy, A. Torrents, H. De Clippeleir, Investigating the dynamics of volatile sulfur compound emission from primary systems at a water resource recovery facility, Water Environ. Res. 93 (2021), https://doi.org/10.1002/wer.1417.
[15] G. Jiang, A. Keating, S. Corrie, K. O'halloran, L. Nguyen, Z. Yuan, Dosing free nitrous acid for sulfide control in sewers: results of field trials in Australia, Water Res. 47 (2013), https://doi.org/10.1016/j.watres.2013.05.024.
[16] R. Lebrero, L. Bouchy, R. Stuetz, R. Muñoz, Odor assessment and management in wastewater treatment plants: a review, Crit. Rev. Environ. Sci. Technol. 41 (2011), https://doi.org/10.1080/10643380903300000.
[17] M.T. Piccardo, M. Geretto, A. Pulliero, A. Izzotti, Odor emissions: a public health concern for health risk perception, Environ. Res. 204 (2022), https://doi.org/10.1016/j.envres.2021.112121.
[18] D. Kasperczyk, K. Urbaniec, K. Barbusinski, E.R. Rene, R.F. Colmenares-Quintero, Application of a compact trickle-bed bioreactor for the removal of odor and volatile organic compounds emitted from a wastewater treatment plant, J. Environ. Manage. 236 (2019), https://doi.org/10.1016/j.jenvman.2019.01.106.
[19] F. Carrera-Chapela, A. Donoso-Bravo, J.A. Souto, G. Ruiz-Filippi, Modeling the odor generation in WWTP: an integrated approach review, Water Air Soil Pollut. 225 (2014), https://doi.org/10.1007/s11270-014-1932-y.
[20] R.M. Fisher, N. Le-Minh, J.P. Alvarez-Gaitan, S.J. Moore, R.M. Stuetz, Emissions of volatile sulfur compounds (VSCs) throughout wastewater biosolids processing, Sci. Total Environ. 616–617 (2018), https://doi.org/10.1016/j.scitotenv.2017.10.282.
[21] J. Sun, S. Hu, K.R. Sharma, B.J. Ni, Z. Yuan, Stratified microbial structure and activity in sulfide- and methane- producing anaerobic sewer biofilms, Appl. Environ. Microbiol. 80 (2014), https://doi.org/10.1128/AEM.02146-14.
[22] G. Bitton, Wastewater Microbiology, Fourth edition, 2010, https://doi.org/10.1002/9780470901243.

[23] M. Yoshimura, Y. Nakano, Y. Yamashita, T. Oho, T. Saito, T. Koga, Formation of methyl mercaptan from L-methionine by *Porphyromonas gingivalis*, Infect. Immun. 68 (2000), https://doi.org/10.1128/IAI.68.12.6912-6916.2000.
[24] D.J. Batstone, J. Keller, I. Angelidaki, S.V. Kalyuzhnyi, S.G. Pavlostathis, A. Rozzi, W.T.M. Sanders, H. Siegrist, Anaerobic Digestion Model No. 1, IWA Publishing, London, 2002.
[25] P. Stellacci, L. Liberti, M. Notarnicola, C.N. Haas, Hygienic sustainability of site location of wastewater treatment plants. A case study. I. Estimating odour emission impact, Desalination 253 (2010), https://doi.org/10.1016/j.desal.2009.11.034.
[26] T. Zarra, V. Naddeo, V. Belgiorno, M. Reiser, M. Kranert, Odour monitoring of small wastewater treatment plant located in sensitive environment, Water Sci. Technol. 58 (2008), https://doi.org/10.2166/wst.2008.330.
[27] A. Eldyasti, G. Nakhla, J. Zhu, Development of a calibration protocol and identification of the most sensitive parameters for the particulate biofilm models used in biological wastewater treatment, Bioresour. Technol. 111 (2012), https://doi.org/10.1016/j.biortech.2012.02.021.
[28] T. Hvitved-Jacobsen, J. Vollertsen, N. Tanaka, An integrated aerobic/anaerobic approach for prediction of sulfide formation in sewers, Water Sci. Technol. (2000), https://doi.org/10.2166/wst.2000.0099.
[29] S. Abdul-Talib, Z. Ujang, J. Vollertsen, T. Hvitved-Jacobsen, Model concept for nitrate and nitrite utilization during anoxic transformation in the bulk water phase of municipal wastewater under sewer conditions, Water Sci. Technol. 52 (2005), https://doi.org/10.2166/wst.2005.0075.
[30] C. Yongsiri, T. Hvitved-Jacobsen, J. Vollertsen, N. Tanaka, Introducing the emission process of hydrogen sulfide to a sewer process model (WATS), Water Sci. Technol. (2003), https://doi.org/10.2166/wst.2003.0227.
[31] K.R. Sharma, Z. Yuan, D. de Haas, G. Hamilton, S. Corrie, J. Keller, Dynamics and dynamic modelling of H2S production in sewer systems, Water Res. 42 (2008), https://doi.org/10.1016/j.watres.2008.02.013.
[32] A. Guisasola, K.R. Sharma, J. Keller, Z. Yuan, Development of a model for assessing methane formation in rising main sewers, Water Res. 43 (2009), https://doi.org/10.1016/j.watres.2009.03.040.
[33] J. Mohanakrishnan, K.R. Sharma, R.L. Meyer, G. Hamilton, J. Keller, Z. Yuan, Variation in biofilm structure and activity along the length of a rising Main sewer, Water Environ. Res. 81 (2009), https://doi.org/10.2175/106143008x390771.
[34] O. Auguet, M. Pijuan, J. Batista, C.M. Borrego, O. Gutierrez, Changes in microbial biofilm communities during colonization of sewer systems, Appl. Environ. Microbiol. 81 (2015), https://doi.org/10.1128/AEM.01538-15.
[35] P. Jin, X. Shi, G. Sun, L. Yang, Y. Cai, X.C. Wang, Co-variation between distribution of microbial communities and biological Metabolization of organics in urban sewer systems, Environ. Sci. Technol. 52 (2018), https://doi.org/10.1021/acs.est.7b05121.
[36] F. Zan, Z. Liang, F. Jiang, J. Dai, G. Chen, Effects of food waste addition on biofilm formation and sulfide production in a gravity sewer, Water Res. 157 (2019), https://doi.org/10.1016/j.watres.2019.03.061.
[37] J. Sun, X. Dai, Q. Wang, Y. Pan, B.J. Ni, Modelling methane production and sulfate reduction in anaerobic granular sludge reactor with ethanol as Electron donor, Sci. Rep. 6 (2016), https://doi.org/10.1038/srep35312.
[38] B. D'Acunto, G. Esposito, L. Frunzo, F. Pirozzi, Dynamic modeling of sulfate reducing biofilms, Comput. Math. Appl. 62 (2011), https://doi.org/10.1016/j.camwa.2011.07.064.
[39] F. Jiang, D.H. wai Leung, S. Li, G.H. Chen, S. Okabe, M.C.M. van Loosdrecht, A biofilm model for prediction of pollutant transformation in sewers, Water Res. 43 (2009), https://doi.org/10.1016/j.watres.2009.04.043.
[40] N. Jourdan, T. Neveux, O. Potier, M. Kanniche, J. Wicks, I. Nopens, U. Rehman, Y. Le Moullec, Compartmental modelling in chemical engineering: a critical review, Chem. Eng. Sci. 210 (2019), https://doi.org/10.1016/j.ces.2019.115196.
[41] J. Haag, C. Gentric, C. Lemaitre, J.P. Leclerc, Modelling of chemical reactors: from systemic approach to compartmental modelling, Int. J. Chem. React. Eng. 16 (2018), https://doi.org/10.1515/ijcre-2017-0172.
[42] J.P. Boltz, B.F. Smets, B.E. Rittmann, M.C.M. Van Loosdrecht, E. Morgenroth, G. T. Daigger, From biofilm ecology to reactors: a focused review, Water Sci. Technol. 75 (2017), https://doi.org/10.2166/wst.2017.061.
[43] M. Krsmanovic, D. Biswas, H. Ali, A. Kumar, R. Ghosh, A.K. Dickerson, Hydrodynamics and surface properties influence biofilm proliferation, Adv. Colloid Interface Sci. 288 (2021), https://doi.org/10.1016/j.cis.2020.102336.
[44] C. Rosen, U. Jeppsson, Aspects on ADM1 Implementation within the BSM2 Framework, Technical Report, 2006.
[45] W.J. Parker, G.H. Wu, Modifying ADM1 to include formation and emission of odourants, Water Sci. Technol. 54 (2006), https://doi.org/10.2166/wst.2006.532.
[46] J.V. da Silva Neto, M.L.C. Elaiuy, E.A.A. Nour, ADM1 approach to the performance optimisation and biogas H2S prediction of a large-scale anaerobic reactor fed on sugarcane vinasse, Water Sci. Technol. 80 (2019), https://doi.org/10.2166/wst.2019.434.
[47] E.L. Barrera, H. Spanjers, K. Solon, Y. Amerlinck, I. Nopens, J. Dewulf, Modeling the anaerobic digestion of cane-molasses vinasse: Extension of the Anaerobic Digestion Model No. 1 (ADM1) with sulfate reduction for a very high strength and sulfate rich wastewater, Water Res. 71 (2015), https://doi.org/10.1016/j.watres.2014.12.026.
[48] K. Sharma, O. Gutierrez, Z. Yuan, M.R.J. Daelman, M.C.M. van Loosdrecht, E.I. P. Volcke, Modelling of methane production and emissions, in: L. Ye, J. Porro, I. Nopens (Eds.), Quantification and Modelling of Fugitive Greenhouse Gas Emissions from Urban Water Systems: A Report from the IWA Task Group on GHG, 2022, https://doi.org/10.2166/9781789060461_197.
[49] M. Kim, M. Zaman, E. Jang, G. Nakhla, M. Ward, O. Gutierrez, J. Willis, J. Walton, D. Santoro, Experimental investigation on hydrogen sulfide production, wastewater characteristics and microbial ecology profiles in anaerobic sewer lines using a sewer physical twin, J. Environ. Chem. Eng. 12 (2024), https://doi.org/10.1016/j.jece.2024.111965.
[50] O. Wanner, W. Gujer, A multispecies Biofilrn model 0, Biotechnol. Bioeng. 28 (1986).
[51] J.P. Boltz, E. Morgenroth, D. Sen, Mathematical modelling of biofilms and biofilm reactors for engineering design, Water Sci. Technol. 62 (2010), https://doi.org/10.2166/wst.2010.076.
[52] M.C. Mussati, P. Aguirre, M. Fuentes, N. Scenna, Aspects on methanogenic biofilm reactor modeling, Lat. Am. Appl. Res. 36 (2006).
[53] M.C.M. Van Loosdrecht, M. Henze, Maintenance, endogeneous respiration, lysis, decay and predation, Water Sci. Technol. (1999), https://doi.org/10.1016/S0273-1223(98)00780-X.
[54] M.S.I. Mozumder, C. Picioreanu, M.C.M. Van Loosdrecht, E.I.P. Volcke, Effect of heterotrophic growth on autotrophic nitrogen removal in a granular sludge reactor, Environ. Technol. (United Kingdom) 35 (2014), https://doi.org/10.1080/09593330.2013.859711.
[55] L. Pokorna-Krayzelova, K.E. Mampaey, T.P.W. Vannecke, J. Bartacek, P. Jenicek, E. I.P. Volcke, Model-based optimization of microaeration for biogas desulfurization in UASB reactors, Biochem. Eng. J. 125 (2017), https://doi.org/10.1016/j.bej.2017.06.009.
[56] V. Fedorovich, P. Lens, S. Kalyuzhnyi, Extension of anaerobic digestion model no. 1 with processes of sulfate reduction, Appl. Biochem. Biotechnol. - A Enzyme Eng. Biotechnol. (1-3) (2003) 33, https://doi.org/10.1385/ABAB:109.
[57] I.R. Ramsay, Modelling and Control of High-Rate Anaerobic Wastewater Treatment Systems, The University of Queensland, 1997, https://doi.org/10.14264/307817.
[58] C. Huiliñir, E. Aspé, M. Roeckel, Modeling of the denitrification/anaerobic digestion process of salmon fishery wastewater in a biofilm tubular reactor, J. Environ. Manage. 92 (2011), https://doi.org/10.1016/j.jenvman.2011.01.015.
[59] C. Huiliñir, E. Aspé, M. Roeckel, Model of simultaneous denitrification and methanogenesis in an upflow packed-bed biofilm reactor: nitrogen compounds' inhibition and pseudo two-dimensional biofilm model, J. Chem. Technol. Biotechnol. 84 (2009), https://doi.org/10.1002/jctb.2033.
[60] H. Eberl, E. Morgenroth, D. Noguera, C. Picioreanu, B. Rittmann, M. Van Loosdrecht, Mathematical modeling of biofilms IWA task group on biofilm modeling, Group (New York) 11, 2006, p. 127.
[61] B.E. Rittmann, J.P. Boltz, D. Brockmann, G.T. Daigger, E. Morgenroth, K. H. Sørensen, I. Takács, M. Van Loosdrecht, P.A. Vanrolleghem, A framework for good biofilm reactor modeling practice (GBRMP), Water Sci. Technol. 77 (2018), https://doi.org/10.2166/wst.2018.021.
[62] F. Zan, G. Guo, T. Zheng, G. Chen, Biofilm development in a pilot-scale gravity sewer: physical characteristics, microstructure, and microbial communities, Environ. Res. 195 (2021), https://doi.org/10.1016/j.envres.2021.110838.
[63] S.G. Pavlostathis, E. Giraldo-Gomez, Kinetics of anaerobic treatment: a critical review, Crit. Rev. Environ. Control. 21 (1991) 411–490, https://doi.org/10.1080/10643389109388424.
[64] G. Tchobanoglous, F.L. Burton, D.H. Stensel, Metcalf &Eddy: Wastewater Engineering: Treatment and Reuse, McGraw Hill Companies, Inc., 2014.
[65] H. Siegrist, D. Vogt, J.L. Garcia-Heras, W. Gujer, Mathematical model for meso- and thermophilic anaerobic sewage sludge digestion, Environ. Sci. Technol. 36 (2002), https://doi.org/10.1021/es010139p.
[66] G.W. Corder, D.I. Foreman, Nonparametric Statistics for Non-Statisticians: A Step-by-Step Approach, 2011, https://doi.org/10.1002/9781118165881.
[67] H. César, M. Silvio, Modeling of an anoxic/methanogenic biofilm: effect of pH calculation within the biofilm, Bioprocess Biosyst. Eng. 36 (2013), https://doi.org/10.1007/s00449-013-0942-2.
[68] W. Ahmed, J. Rodríguez, Modelling sulfate reduction in anaerobic digestion: complexity evaluation and parameter calibration, Water Res. 130 (2018), https://doi.org/10.1016/j.watres.2017.11.064.
[69] V. Fedorovich, P. Lens, S. Kalyuzhnyi, Extension of Anaerobic Digestion Model No. 1 with processes of sulfate reduction, Appl. Biochem. Biotechnol. 109 (2003) 33–45.
[70] G.H. Wu, Modelling Formation and Emission of Odourous Compounds in Anaerobic Digesters, Masters of Applied Science, Carleton University, 2004.
[71] S. Kalyuzhnyi, V. Fedorovich, Integrated mathematical model of UASB reactor for competition between sulphate reduction and methanogenesis, Water Sci. Technol. 36 (6–7) (1997) 201–208, https://doi.org/10.1016/S0273-1223(97)00524-6.
[72] P.S. Stewart, Diffusion in biofilms, J. Bacteriol. 185 (2003) 1485–1491, https://doi.org/10.1128/JB.185.5.1485-1491.2003.
[73] D.R. ed Lide, CRC Handbook of Chemistry and Physics, CRC Press, 2014, https://doi.org/10.1201/b17118.
[74] R. Sander, Compilation of Henry's Law constants (version 4.0) for water as solvent, Atmos. Chem. Phys. 15 (2015), https://doi.org/10.5194/acp-15-4399-2015.
[75] X. Flores-Alsina, K. Solon, C. Kazadi Mbamba, S. Tait, K.V. Gernaey, U. Jeppsson, D.J. Batstone, Modelling phosphorus (P), sulfur (S) and iron (Fe) interactions for dynamic simulations of anaerobic digestion processes, Water Res. 95 (2016), https://doi.org/10.1016/j.watres.2016.03.012.

[76] K. Bilyk, I. Takács, J. Rohrbacher, P. Pitt, R. Latimer, P. Dold, Full-scale dynamic testing advances fundamental understanding of denitrification filters, Proc. Water Environ. Fed. 2008 (2012), https://doi.org/10.2175/193864708788735718.
[77] G. Sin, J. Weijma, H. Spanjers, I. Nopens, Dynamic model development and validation for a nitrifying moving bed biofilter: effect of temperature and influent load on the performance, Process Biochem. 43 (2008), https://doi.org/10.1016/j.procbio.2008.01.009.
[78] D.J. Batstone, Mathematical modelling of anaerobic reactors treating domestic wastewater: rational criteria for model use, Rev. Environ. Sci. Biotechnol. 5 (2006), https://doi.org/10.1007/s11157-005-7191-z.
[79] Y. Li, J. Jiang, W. Zhang, G. Yang, Changes in stoichiometric ratio of carbon and sulfate affect methanogenesis pathways in sulfate-rich sewers, J. Clean. Prod. 426 (2023), https://doi.org/10.1016/j.jclepro.2023.139112.
[80] V. Blanes-Vidal, S.G. Sommer, E.S. Nadimi, Modelling surface pH and emissions of hydrogen sulphide, ammonia, acetic acid and carbon dioxide from a pig waste lagoon, Biosyst. Eng. 104 (2009), https://doi.org/10.1016/j.biosystemseng.2009.09.008.